

Selection of Software for Mechanical Engineering Undergraduates

*C.T. Cheah (Australia), C. S. Yin (Australia), T Halim (Australia), Aaron
Blicblau (Australia)*

Abstract

With the growing complexity of engineering problems and advancement of computer hardware, computational skills have become a necessary tool for engineers. Despite the importance of computational skills, not all the subjects in mechanical engineering curriculum at our university are integrated with computational skills. In some subjects where computati have a long learning curve and not used consistently throughout the curriculum. The current software packages that are being used are one of the best in their respective categories. Even though these software packages are robust, they are not user-friendly, time consuming and are more suitable for postgraduate research level rather than undergraduate studies.

Keywords: Software packages, computational analysis, student learning



6th BSME International Conference on Thermal Engineering (ICTE 2014)

Experimental investigation on friction coefficient of composite materials sliding against SS 201 and SS 301 counterfaces

Dewan Muhammad Nuruzzaman^a, Mohammad Asaduzzaman Chowdhury^{b*},
Md. Mostafizur Rahman^b, Md. Arefin Kowser^b and Biplov Kumar Roy^b

^a*Faculty of Manufacturing Engineering, University Malaysia Pahang (UMP), Malaysia*

^b*Department of Mechanical Engineering, Dhaka University of Engineering and Technology (DUET), Gazipur-1700, Bangladesh*

Abstract

In this research, friction coefficients of composite materials such as gear fiber reinforced plastic (gear fiber) and glass fiber reinforced plastic (glass fiber) are investigated and compared. In the experiments, gear fiber and glass fiber slide against different austenitic stainless steels such as stainless steel 201 (SS 201) and stainless steel 301 (SS 301). Experiments are carried out at low loads 2, 4 and 6 N, low sliding velocities 0.2, 0.4 and 0.6 m/s and relative humidity 70%. The obtained results reveal that in general, friction coefficient of gear fiber and glass fiber increases with the increase in normal load and sliding velocity. Results show that friction coefficient of glass fiber-SS 201 pair is the highest and gear fiber-SS 301 pair is the lowest within the observed range of normal load and sliding velocity. On the other hand, it is found that friction coefficient of glass fiber-SS 301 pair is slightly higher than that of gear fiber-SS 201 pair. During the running-in process, friction coefficient of gear fiber and glass fiber steadily increases with the increase in rubbing time and after certain duration of rubbing, it remains constant regardless of the counterface material. The obtained results reveal that for the observed range, the influence of normal load on the frictional properties of gear fiber and glass fiber is greater than that of sliding velocity. At identical operating conditions, the magnitudes of friction coefficient of gear fiber and glass fiber are different depending on normal load, sliding velocity and counterface material.

© 2015 The Authors. Published by Elsevier Ltd.

Peer-review under responsibility of organizing committee of the 6th BSME International Conference on Thermal Engineering (ICTE 2014).

Keywords: Friction coefficient; gear fiber; glass fiber; SS 201; SS 301; normal load; sliding velocity; running-in process

* Corresponding author. Tel.: +88- 01766589508; fax: +88-924703.

E-mail address: asadzmn2014@yahoo.com

1. Introduction

In the past decade, a number of investigations were carried out on friction and wear of different type materials under different operating conditions. Several researchers [1-7] reported that friction and wear of metals, polymers and composites rubbing against metal depend on several parameters such as normal load, roughness of the rubbing surfaces, sliding velocity, relative humidity, lubrication etc. Among these parameters, normal load and sliding velocity are the most influential parameters that dictate the tribological properties of the materials. Friction coefficient of polymers and its composites sliding against metal increase or decrease depending on the range of operating conditions and sliding pairs. There have been also investigations to explore the influence of type of material, relative motion and frequency, amplitude and direction of vibration [8-10]. It was reported that the influence of velocity on the sliding wear of polymer and its composite is greater than that of applied load [11] although other researchers have different views [12,13]. Tribological performance of polymeric material can be improved significantly by the incorporation of fiber reinforcement or fillers. Friction and wear characteristics of polymers and composite materials sliding against rough steel counterface were investigated [14] and it was reported that frictional values of these polymers and composites are significantly influenced by the applied load and duration of rubbing. Wear rates of these polymers and composites are also greatly influenced by the applied normal load. The influence of sliding velocity on the friction and wear of polymer and composite materials sliding against rough steel counterface were also investigated [15]. The obtained results showed that in general, friction coefficient increases with the increase in sliding velocity for all the tested materials. It was also found that wear rates of these polymer and composite materials are significantly influenced by sliding velocity. After friction process, it was observed that surface roughnesses of these materials are greatly changed depending on sliding velocity. Friction coefficient and wear rate of different composite materials sliding against smooth and rough mild steel counterfaces were investigated [16]. It was found that the friction coefficient and wear rate of these materials are significantly influenced by the applied normal load, sliding velocity and counterface surface condition.

Despite the aforementioned research works, frictional properties of different composites such as gear fiber and glass fiber sliding against different grades of austenitic stainless steels under different normal loads and sliding velocities are yet to be clearly understood. Therefore, in this study, the frictional properties of gear fiber and glass fiber sliding against stainless steel 201 (SS 201) and stainless steel 301 (SS 301) under low load and low velocity conditions are investigated. The influence of rubbing time on friction coefficient of these composite materials is also examined. Nowadays, different composite-steel combinations are widely used for sliding/rolling applications where low friction is required. Due to these tribological applications, different material combinations have been selected in this research study.

2. Experimental

Experiments are carried out using a pin-on-disc set-up which is shown in Fig. 1. A cylindrical pin (both ends flat) can slide on a horizontal surface (disc) which rotates using the power from a motor. A circular test disc is fixed on a horizontal plate which can rotate and this rotation (rpm) can be varied by an electronic speed control unit. A vertical shaft which connects the horizontal plate with a stainless steel base plate. To provide the alignment and rigidity to the main structure of this set-up, four vertical cylindrical bars are rigidly fixed around the periphery to connect horizontal plate with the stainless steel base plate. The whole set-up is placed on a main base plate which is made of mild steel (10 mm thick). The mild steel main base plate is supported by a rubber block (20 mm thick) at the lower side. A rubber sheet (3 mm thick) is also placed at the upper side of the main base plate to absorb any vibration during the friction test. For power transmission from the motor to the stainless steel base plate, a compound V-pulley is fixed with the shaft. A cylindrical pin (6 mm diameter) made of stainless steel can be fitted in a holder and this holder is subsequently fixed by an arm. A load cell (CLS-10NA) along with digital indicator (TD-93A) was used to measure the frictional force. To obtain the friction coefficient, the measured frictional force was divided by the applied normal load. To measure the roughness, A precision roughness checker was used. Each experiment was carried out for 30 minutes and after each experiment, new pin and new test sample were used. Each experiment was repeated five times to ensure the reliability of test results and the average value was taken into consideration. Table 1 shows the detail of the experimental conditions.

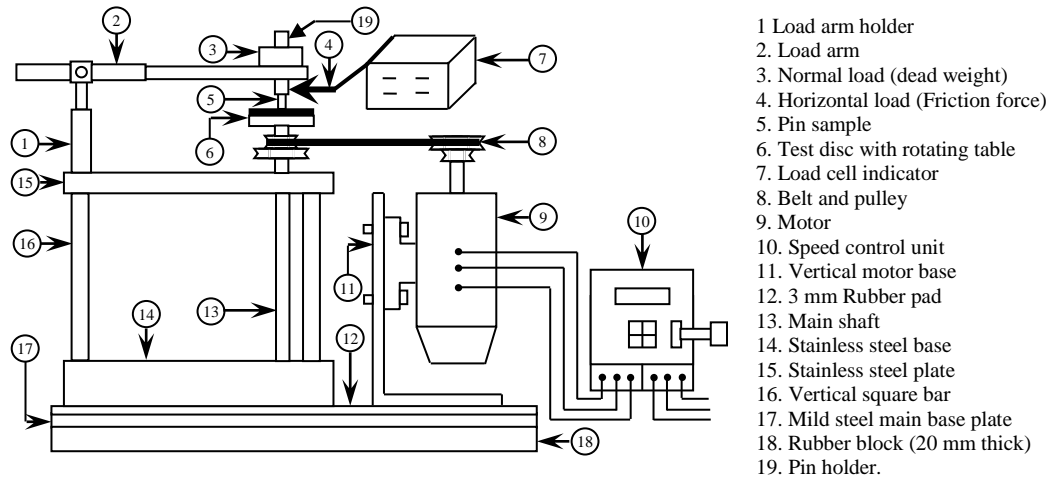


Fig. 1. Block diagram of the pin-on-disc experimental set-up

Table 1. Experimental conditions

Sl. No.	Parameters	Operating conditions
1.	Normal Load	2, 4, 6 N
2.	Sliding Velocity	0.2, 0.4, 0.6 m/s
3.	Relative Humidity	70 (\pm 5)%
4.	Duration of Rubbing	30 minutes
5.	Surface Condition	Dry
6.	Disc material	(i) Gear fiber (ii) Glass fiber
7.	Average Surface Roughness of Gear fiber and Glass fiber, R_a	0.4-0.5 μ m
8.	Counterface pin material	(i) SS 201 (ii) SS 301
9.	Average Surface Roughness of SS 201 and SS 301, R_a	0.2-0.3 μ m

3. Results and discussion

Fig. 2 shows the variation of friction coefficient during the running-in process at different normal loads 2, 4 and 6 N. Experiments were carried out at sliding velocity 0.4 m/s. In the experiments, gear fiber was used for disc material and SS 201 was used for counterface pin material. Curve 1 for normal load 2 N shows that at early stage of rubbing, friction coefficient of gear fiber is about 0.025 and after that it increases very steadily up to 0.05. It was observed that friction coefficient becomes steady over a duration of 24 minutes and it remains constant for the rest of the experimental time. It is believed that due to the ploughing effect, trapped wear particles between the contacting surfaces and surface roughening of the disc, friction force increases with rubbing time. After the running-in process for a certain duration, surface roughness and other parameters reached to a steady state value and there is no change in friction with time. Curves 2 and 3 show the results for normal load 4 and 6 N respectively and the trends of variation of friction coefficient are almost similar as that of curve 1. It was observed that gear fiber disc takes different time to stabilize which is 24, 20 and 17 minutes for different normal loads 2, 4 and 6 N respectively. It indicates that time to reach steady friction is less as the normal load is increased. This is because the surface roughness and other parameter attain a steady level at a shorter period of time with the increase in normal load.

Variations of friction coefficient with duration of rubbing are shown in Fig. 3 and in the experiments, glass fiber was used as disc material and SS 201 was used as pin material. It is observed that at 2 N normal load (curve 1), friction coefficient is 0.046 at initial stage of rubbing and after that friction coefficient increases steadily up to 0.071 which remains almost constant till experimental time 30 minutes. For normal load 4 and 6 N (curves 2 and 3), the trends of variation of friction coefficient are almost similar as that of curve 1. It is also observed that glass fiber disc takes about 25, 21 and 20 minutes to stabilize when the applied normal load is 2, 4 and 6 N respectively. During the running-in process, glass fiber disc takes less time to reach steady state friction when higher load is applied.

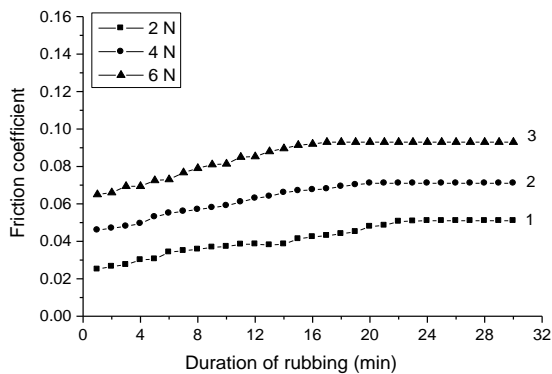


Fig. 2. Variation of friction coefficient with duration of rubbing at different normal loads (Sliding velocity: 0.4 m/s, test sample: gear fiber, pin: SS 201)

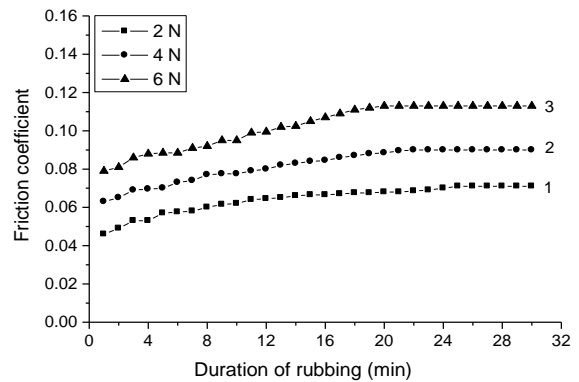


Fig. 3. Variation of friction coefficient with duration of rubbing at different normal loads (Sliding velocity: 0.4 m/s, test sample: glass fiber, pin: SS 201)

Fig. 4 shows the variations of friction coefficient with duration of rubbing at different loads and in the experiments, gear fiber was used as disc material and SS 301 was used as counterface pin material. Curve 1 at 2 N normal load shows that during initial rubbing, friction coefficient is 0.021 which rises for a certain duration of rubbing to a value of 0.035 and then it becomes steady for the rest of the experimental time. Almost similar trends of variation are observed in curves 2 and 3 which are drawn for load 4 and 6 N respectively. From these curves, it can be observed that time to reach steady friction is different for different normal loads. The obtained results show that at normal load 2, 4 and 6 N, gear fiber takes 25, 21 and 18 minutes respectively to reach steady friction. It is apparent that higher the normal load, gear fiber takes less time to stabilize. Experiments were carried out to observe the variation of friction coefficient at different normal loads when glass fiber disc slid against SS 301 pin and the results are shown in Fig. 5. Curve 1 for normal load 2 N shows that during initial rubbing, friction coefficient is 0.034 which increases almost linearly up to 0.055 over a duration of 25 minutes and after that it remains steady. Curves 2 and 3 for normal load 4 and 6 N show similar trends as that of curve 1. During the running-in process, glass fiber disc takes 25, 22 and 18 minutes to stabilize when applied normal load 2, 4 and 6 N respectively.

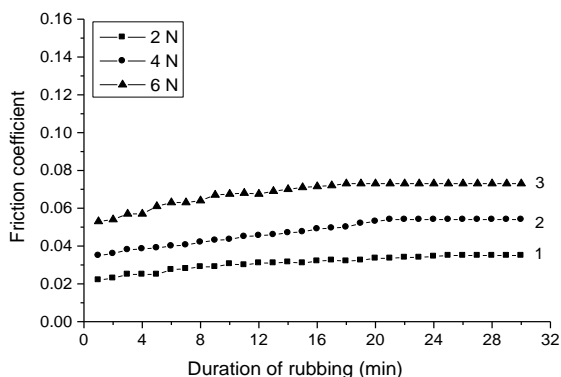


Fig. 4. Variation of friction coefficient with duration of rubbing at different normal loads (Sliding velocity: 0.4 m/s, test sample: gear fiber, pin: SS 301)

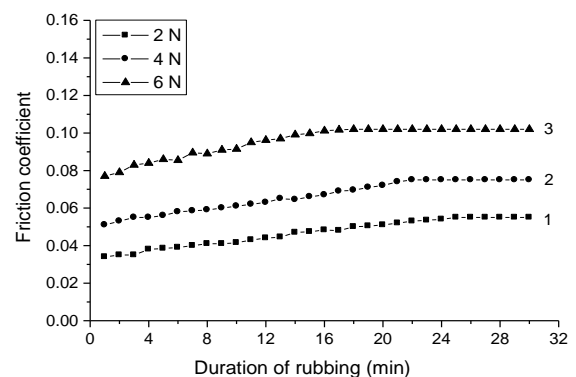


Fig. 5. Variation of friction coefficient with duration of rubbing at different normal loads (Sliding velocity: 0.4 m/s, test sample: glass fiber, pin: SS 301)

Figure 6 shows a comparison of friction coefficient of different composite-stainless steel pairs at different normal loads. Results show that friction coefficient varies from 0.05 to 0.093, 0.071 to 0.113, 0.035 to 0.073 and 0.055 to 0.1 for gear fiber-SS 201, glass fiber-SS 201, gear fiber-SS 301 and glass fiber-SS 301 pairs respectively due to the variation of normal load from 2 to 6 N. These friction results are obtained from the steady values of friction coefficient of Figs. 2, 3, 4 and 5 respectively. It is apparent that friction coefficient increases almost linearly with the increase in normal load for all the material combinations. It is believed that because of more ploughing effect which causes roughening of the disc surface, friction coefficient increases with the increase in normal load. From the figure it is apparent that within the observed range of normal load, friction coefficient of glass fiber-SS 201 pair is the highest and gear fiber-SS 301 pair is the lowest. It is also observed that frictional values of glass fiber-SS 301 and gear fiber-SS 201 pairs are in between the highest and lowest values. On the other hand, glass fiber-SS 301 pair shows higher friction than gear fiber-SS 201 pair. This is because at higher normal load, hardness of SS 201 and glass fiber might have significant role on the friction process. After the running-in process, average surface roughness (R_a) was measured which varied from 1.1-1.45 μm , 1.35-1.7 μm , 0.95-1.25 μm and 1.15-1.57 μm for gear fiber-SS 201, glass fiber-SS 201, gear fiber-SS 301 and glass fiber-SS 301 pairs respectively.

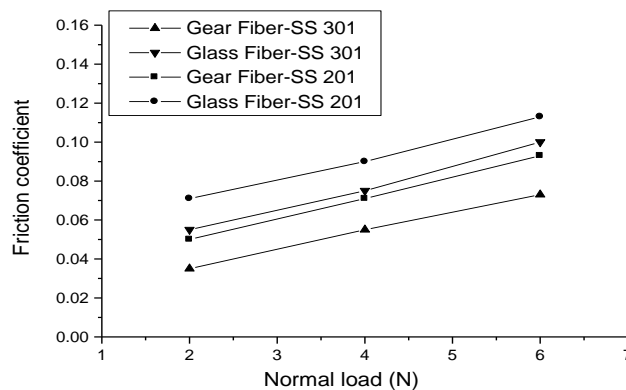


Fig. 6. Comparison of friction coefficient of different composite-stainless steel pairs at different normal loads (Sliding velocity: 0.4 m/s)

Variations of friction coefficient with duration of rubbing at different sliding velocities are shown in Fig. 7 and in this case, gear fiber disc slid against SS 201 pin. Curves 1, 2 and 3 show the results for sliding velocity 0.2, 0.4 and 0.6 m/s respectively. Curve 1 shows that at initial rubbing, friction coefficient is 0.036 which increases steadily up to 0.06 over a duration of 23 minutes and after that it remains steady. Curves 2 and 3 show that the trends in variation of friction coefficient are almost same as that of curve 1. It is observed that at 0.2, 0.4 and 0.6 m/s, gear fiber takes 23, 20 and 17 minutes respectively to reach steady friction. Variations of friction coefficient with duration of rubbing are presented in Fig. 8 and in this case, glass fiber disc slid against SS 201 pin. Results show that glass fiber takes 23, 21 and 17 minutes to reach steady friction at 0.2, 0.4 and 0.6 m/s respectively. Variations of friction coefficient are also shown in Fig. 9 and in the experiments, gear fiber disc slid against SS 301 counterface. These results show that for higher sliding velocity, gear fiber takes less time to stabilize. Results of the variations of friction coefficients are shown in Fig. 10 and in this case, glass fiber disc slid against SS 301 counterface. From the obtained results, it is clear that the trends of frictional variation are almost similar but at higher sliding velocity, frictional values are higher and glass fiber takes less time to stabilize.

Figure 11 shows a comparison of friction coefficient of different composite-stainless steel pairs at different sliding velocities. It is shown that friction coefficient varies from 0.06 to 0.082, 0.078 to 0.103, 0.043 to 0.067 and 0.064 to 0.085 for gear fiber-SS 201, glass fiber-SS 201, gear fiber-SS 301 and glass fiber-SS 301 pairs respectively due to the variation of sliding velocity from 0.2 to 0.6 m/s. These results are obtained from the steady frictional values of Figs. 7, 8, 9 and 10 respectively. It can be seen that friction coefficient of all the material pairs increases almost linearly with the increase in sliding velocity. As comparison, frictional values of glass fiber-SS 201 pair are the highest and gear fiber-SS 301 pair are the lowest for the observed range of sliding velocity. It can also be

observed that frictional values of gear fiber-SS 201 and glass fiber-SS 301 pairs are in between the highest and lowest values as before (Fig. 6). On the other hand, glass fiber-SS 301 pair exhibits slightly higher friction than gear fiber-SS 201 pair. After the friction process, average surface roughness (R_a) was measured as 1.23-1.42 μm , 1.38-1.61 μm , 1.03-1.27 μm and 1.24-1.45 μm for gear fiber-SS 201, glass fiber-SS 201, gear fiber-SS 301 and glass fiber-SS 301 pairs respectively. Moreover, as comparison of these results (Fig. 11) with the results of Fig. 6, it reveals that within the observed range, the influence of normal load on the frictional properties of the tested material pairs is greater than that of sliding velocity.

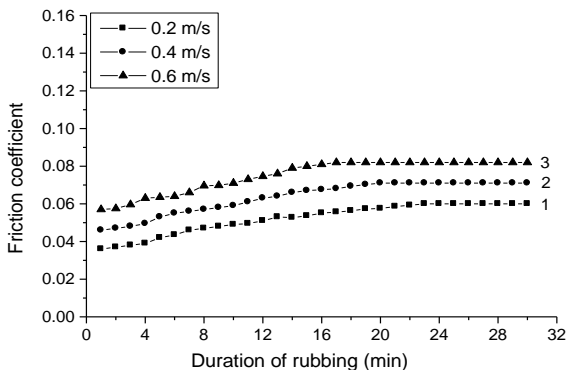


Fig. 7. Variation of friction coefficient with duration of rubbing at different sliding velocities (Normal load: 4 N, test sample: gear fiber, pin: SS 201)

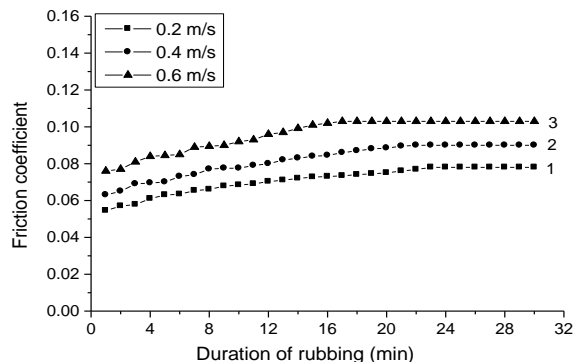


Fig. 8. Variation of friction coefficient with duration of rubbing at different sliding velocities (Normal load: 4 N, test sample: glass fiber, pin: SS 201)

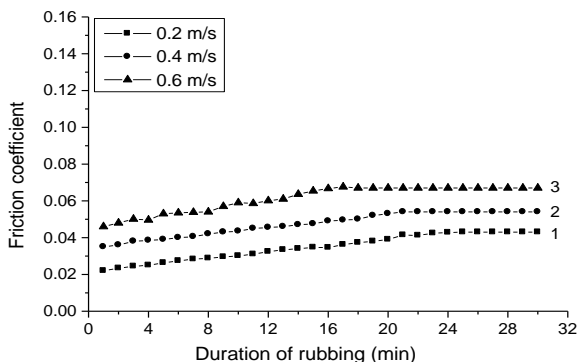


Fig. 9. Variation of friction coefficient with duration of rubbing at different sliding velocities (Normal load: 4 N, test sample: gear fiber, pin: SS 301)

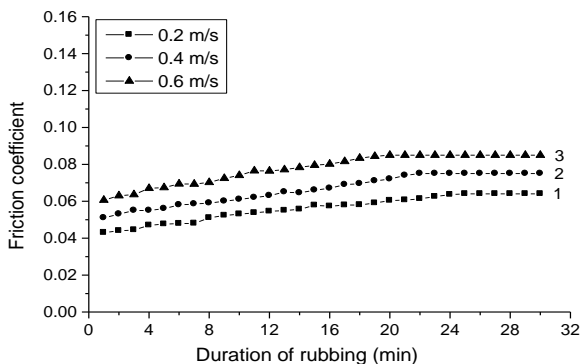


Fig. 10. Variation of friction coefficient with duration of rubbing at different sliding velocities (Normal load: 4 N, test sample: glass fiber, pin: SS 301)

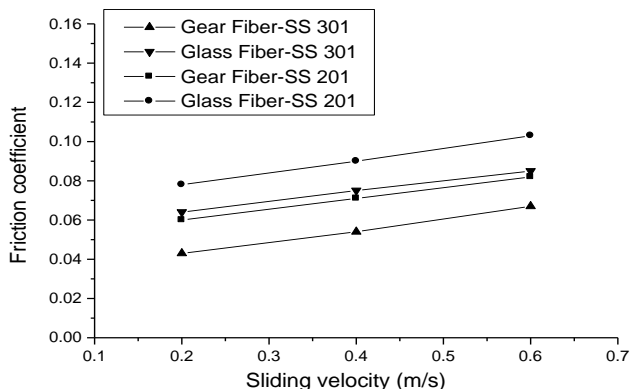


Fig. 11. Comparison of friction coefficient of different composite-stainless steel pairs at different sliding velocities (Normal load: 4 N)

4. Conclusion

From this research study, the obtained results are summarized as:

1. Within the observed range, frictional properties of gear fiber and glass fiber are influenced by normal load, sliding velocity and counterface material. During running-in process, friction coefficient increases with the increase in rubbing time and after a certain duration, it becomes steady for both gear fiber and glass fiber. The obtained results show that during friction process, gear fiber or glass fiber disc takes less time to stabilize as the normal load or sliding velocity increases. Moreover, the time to reach steady friction is different for gear fiber or glass fiber depending on applied normal load or sliding velocity.
2. Under low load and low velocity conditions, in general, friction coefficient increases with the increase in normal load or sliding velocity for all the material pairs. At identical operating conditions, friction coefficient of glass fiber-SS 201 pair is the highest whereas gear fiber-SS 301 pair shows the lowest friction coefficient. Moreover, the frictional values of glass fiber-SS 301 pair are slightly higher than that of gear fiber-SS 201 pair.
3. Regardless of the counterface material, the influence of normal load on the frictional properties of gear fiber and glass fiber is greater than that of sliding velocity.

Therefore, maintaining an appropriate level of normal load, sliding velocity as well as appropriate choice of material pair, friction can be kept to some lower value to improve the mechanical processes in order to ensure performance and quality in industry.

References

- [1] A. Mimaroglu, H. Unal, T. Arda, Friction and wear performance of pure and glass fiber reinforced poly-ether-imide on polymer and steel counterface materials, *Wear*, 262 (2007) 1407–1413.
- [2] B. Suresha, G. Chandramohan, P. Samapthkumaran, S. Seetharamu, S. Vynatheya, Friction and wear characteristics of carbon-epoxy and glass-epoxy woven roving fiber composites. *J. Reinf. Plast. Comp.* 25 (2006) 771-782.
- [3] N.S.M. El-Tayeb, B.F. Yousif, T.C. Yap, Tribological studies of polyester reinforced with CSM 450-R-glass fiber sliding against smooth stainless steel counterface. *Wear* 261 (2006) 443–452.
- [4] Yu. Sirong, Yu. Zhongzhen, Yiu-Wing Mai. Effects of SEBS-g-MA on tribological behavior of nylon 66/organoclay nanocomposites. *Tribol. Int.* 40 (2007) 855 – 862.
- [5] J. Wang, M. Gu, S. Bai, S. Ge, Investigation of the influence of MoS₂ filler on the tribological properties of carbon fiber reinforced nylon 1010 composites. *Wear* 255 (2003) 774–779.
- [6] J. Wang, M. Gu, Wear properties and mechanisms of nylon and carbon-fiber-reinforced nylon in dry and wet conditions. *J. Appl. Polym. Sci.* 93 (2004) 789–795.
- [7] M.A.Chowdhury, D.M. Nuruzzaman, Experimental Investigation on Friction and Wear Properties of Different Steel Materials. *Tribol. Ind.* 35 (2013) 42-50.
- [8] M.A. Chowdhury, M.M. Helali, The effect of amplitude of vibration on the coefficient of friction for different materials. *Tribol. Int.* 41 (2008) 307 – 314.
- [9] M.A. Chowdhury, M.M. Helali, The frictional behavior of materials under vertical vibration. *Ind. Lubr. Tribol.* 61 (2009) 154 – 160.
- [10] M.A. Chowdhury, M.M. Helali, The frictional behavior of composite materials under horizontal vibration. *Ind. Lubr. Tribol.* 61 (2009) 246 – 253.
- [11] A. Mimaroglu, H. Unal, T. Arda, Friction and wear performance of pure and glass fiber reinforced poly-ether-imide on polymer and steel counterface materials, *Wear*, 262 (2007) 1407–1413.
- [12] H. Unal, A. Mimaroglu, U. Kadioglu, H. Ekiz, Sliding friction and wear behaviour of polytetrafluoroethylene and its composites under dry conditions, *Mater. Des.* 25 (2004) 239–245.
- [13] H. Unal, U. Sen, A. Mimaroglu, An approach to friction and wear properties of polytetrafluoroethylene composite, *Mater. Des.* 27 (2006) 694-699.
- [14] D.M. Nuruzzaman, M.A.Chowdhury, M.L. Rahaman, Effect of duration of rubbing and normal load on friction coefficient for polymer and composite materials, *Ind. Lubr. Tribol.* 63 (2011) 320-326.
- [15] D.M. Nuruzzaman, M.L. Rahaman, M.A. Chowdhury, Friction coefficient and wear rate of polymer and composite materials at different sliding speeds, *Int. J. Surf. Sci. Eng.* 6 (2012) 231-245.
- [16] M.A. Chowdhury, D.M. Nuruzzaman, B.K. Roy, S. Samad, R. Sarker, A.H.M. Rezwan, Experimental Investigation of Friction Coefficient and Wear Rate of Composite Materials Sliding Against Smooth and Rough Mild Steel Counterfaces. *Tribol. Ind.* 35 (2013) 286-296.



6th BSME International Conference on Thermal Engineering (ICTE 2014)

Decolorization of Methyl Orange Using Mill Scale by Photo-Fenton Reaction

Sanjidah Akter Urmi, ASW Kurny & Fahmida Gulshan*

*Materials and Metallurgical Engineering Department
Bangladesh University of Engineering and Technology
Dhaka, Bangladesh*

Abstract

The textile dyeing industries generate large amount of effluents, sewage sludge and solid waste materials everyday which are being directly discharged into the surrounding channel, agricultural fields, irrigation channels, surface water and these finally enter into river. The presence of dyes in surface and subsurface water is making them not only aesthetically objectionable but also causes many water borne diseases. Various options have been being employed to treat such wastes. These include chemical treatment such as chlorination and ozonation, electrochemical treatment, physical treatment such as adsorption by activated carbon and membranes, biological treatment and advanced oxidation processes (AOPs). AOPs have attracted wide interests in wastewater treatment. AOPs are based on the generation of hydroxyl radicals in water, which are highly reactive and next on Selective oxidants being able to oxidize organic compounds particularly unsaturated organic compounds such as azo dyes. Among AOPs, two of the most important processes to generate hydroxyl radicals are using the photo-Fenton and photo-ferrioxalate ($\text{Fe}^{2+}/\text{H}_2\text{O}_2/\text{UV}$ and $\text{Fe}^{2+}/\text{OA}/\text{UV}$) systems. In the present study, the aqueous solution of Methyl Orange (MO), a model organic dye has been subjected to photocatalytic degradation by UV irradiation in presence of mill scale (iron oxide, solid waste generated in steel plants) containing different concentrations of H_2O_2 employing photo-Fenton process. The effect of various parameters such as initial mill scale amount, initial hydrogen peroxide (H_2O_2) concentration & initial dye concentration on decolorization process has been studied. The experiments were carried out by varying amount of mill scale (0.01-0.3 g/100 mL), initial concentration of dye (0.01-0.10 mM/100 mL) and hydrogen peroxide concentration (1-4 mL/100 mL). The optimum mill scale content was found to be 50 mg/100 mL. The degradation rate decreased with increasing dye concentration.

© 2015 The Authors. Published by Elsevier Ltd.

Peer-review under responsibility of organizing committee of the 6th BSME International Conference on Thermal Engineering (ICTE 2014).

Keywords: Photo-fenton, Photocatalytic degradation, Methyl Orange.

*Corresponding author. Tel: +088 01733892419 fax:
E-mail address: fahmidagulshan@mme.buet.ac.bd

1. Introduction

Water pollution i.e. the pollution of water bodies on the planet, is one of the raging environmental issues that our planet is facing today. It occurs when pollutants (e.g. untreated dyes in effluents from dyeing factories and leather industries) are discharged directly or indirectly into water bodies without adequate treatment to remove harmful compounds. From pollution point of view, dyeing, leather, sugar, pulp and paper industries are the major contributors. Due to the complex aromatic structure and stability of these dyes, conventional biological pre-treatment methods are ineffective for degradation. A number of physical and chemical techniques had been reported for the treatment of dye effluent over the past few years. In most cases, the degradation is conducted for dissolved compounds in water with UV radiation. Recently, advanced oxidation processes (AOPs) have been found to be very effective for removing organic pollutants from wastewater [1, 2]. The AOPs involve the generation of hydroxyl radicals (HO^\bullet) which can degrade most organic compounds to carbon dioxide and water due to their high oxidation potential ($E_0 = +2.80 \text{ V}$) [3]. The use of semiconducting materials like iron oxide as a photocatalyst for various chemical reactions are well received due to their unique optoelectronic and photocatalytic properties. For the decomposition of dyes, mill scale with H_2O_2 under UV is considered due to its stability as a support in solution. Among AOPs, two of the most important processes to generate hydroxyl radicals are using the Fenton and photo-Fenton ($\text{Fe}^{2+}/\text{H}_2\text{O}_2$ and $\text{Fe}^{2+}/\text{H}_2\text{O}_2/\text{UV}$) systems [4]. In these reactions, H_2O_2 is added as the direct source of HO^\bullet [5, 6].

The use of $\text{Fe}^{2+}/\text{H}_2\text{O}_2$ as an oxidant for wastewater treatment is attractive since iron is highly abundant and non-toxic, and a 30% H_2O_2 aqueous solution is easy to handle and environmentally not harmful.



In the dark, the reaction is retarded after complete conversion of Fe^{2+} to Fe^{3+} . Thus Organic pollutant degradation rate could be increased by irradiation of Fenton with UV light (Photo - Fenton process). UV light leads not only to the formation of additional hydroxyl radicals but also to the recycling of ferrous catalyst by reduction of Fe^{3+} . In this way, the concentration of Fe^{2+} is increased and the overall reaction is accelerated. It is reported that the removal rate is strongly dependent on the initial concentration of the dye, Fe^{2+} and H_2O_2 [7].

The UV/ H_2O_2 process involves the photolysis of hydrogen peroxide. The most accepted mechanism for this H_2O_2 photolysis is the rupture of the O-O bond by the action of ultraviolet light forming two hydroxyl radicals.



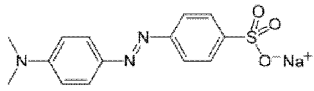
In the present study MO is used as model organic pollutant and its degradation is studied in the presence of mill scale obtained from local steel plant in H_2O_2 solution under UV light.

2. Experimental Details:

2.1. Material

Main reagents were MO, H_2O_2 and mill scale. Mill scale was collected from local steel plant. All other chemicals with analytical grade were purchased. All the chemicals were used without further purification to decompose the dye. Properties of MO are shown in Table 1.

Table 1. Properties of Methyl Orange

Name	Methyl Orange
Wavelength λ_{\max} (nm)	463
Molecular weight (g/mol)	327.334029
Molecular structure	

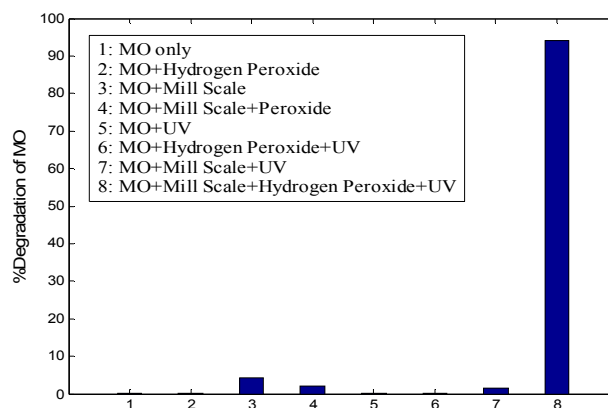
2.2. Procedure

The photo degradation of MO was carried out using two 8W black light lamps with the main emission at 365nm. The sample suspension was formed by adding varying amounts of mill scale to 100 ml of aqueous solution containing MO and H₂O₂. Before photoreaction, the suspension was magnetically stirred in the dark for 30 minute to establish an adsorption-desorption equilibrium. The aqueous suspensions were then illuminated by UV while being magnetically stirred. At the specific time intervals, the analytical samples were withdrawn from the suspension and then stored in the dark for needed analysis. The absorbance spectrum in each experiment was determined from a UV-vis spectrophotometer and the degradation of MO was monitored by recording the absorbance at $\lambda=463$ nm as a function of illumination time.

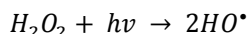
3. Results and Discussion

3.1. Effect of combinations of Mill scale, H₂O₂ and UV

A set of experiments were carried out under different conditions through MO alone, MO + UV, MO + Mill Scale, MO + H₂O₂, MO + Mill Scale+ H₂O₂, MO + UV+ Mill Scale, MO + UV+ H₂O₂, MO + UV+ Mill Scale+ H₂O₂. Figure 1 shows percentage of photodecomposition of MO under these experimental conditions. Solution containing only H₂O₂ shows almost no decomposition of MO after 60 min reaction. UV illumination with H₂O₂ but no mill scale also shows very slight decomposition after 60 min reaction. But combination of mill scale, H₂O₂ and UV shows very fast decomposition (>90% after 60 min).

Fig. 1. Effect of combinations of Mill Scale, H₂O₂ and UV

This is because hydrogen peroxide and UV together, form two free hydroxyl radicals ($\text{HO}\cdot$) which are potent oxidizing agents.

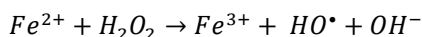


The free hydroxyl radicals are excited state species since they are characterized by one-electron deficiency and are therefore extremely unstable. Because of their instability, they tend to react with the first chemical it comes in contact with. Hydroxyl radicals ($\text{HO}\cdot$) also tend to completely oxidize dissolved organic contaminants in aqueous media and produce carbon dioxide, water and salts as by products. Hydrogen peroxide is catalyzed with UV irradiation to create highly reactive radicals which react rapidly. Therefore the combination results fastest decomposition of MO. The necessity of using this combination is also reported earlier [8]

3.2. Effect of Mill scale concentration in MO decomposition

Equations and formulae Mill scale produces hydroxyl radical which is primary requirement to break the bond of the MO. So we may expect that more amount of mill scale will produce hydroxyl radical as well as the MO degradation. But in practical we found it to be different and got an optimum value. To measure this optimum value a set of experiments were carried out by varying the amount of mill scale from 0.01 g to 0.3 g in 100 ml 0.1 mM MO decomposition.

From the result (shows in figure 2) it is clearly seen that the decomposition of MO is distinctly increased with the increasing amount of mill scale up to 50mg/L. The lesser decomposition capacity of Fe^{2+} at lower concentration might be attributed due to the less hydroxyl radical production [9] which increases with increasing amount of catalyst from 10mg/L to 50mg/L. This is because more $\text{HO}\cdot$ radicals are produced with the increase of Fe^{2+} according to Equation below [10, 11, 12].



With increasing the mill scale amount above 0.05g/L, the decomposition rate again slows down which is clearly shown in Figure 3. This is because excess of Fe^{2+} ions, produced by the photo reduction of Fe^{3+} ions in the solution, compete for the hydroxyl radicals along with the dye molecules and act as hydroxyl radical scavenger [13, 14, 15, 16].

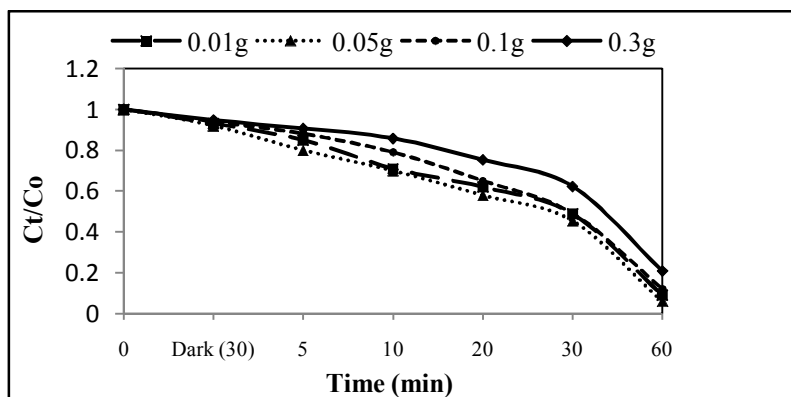


Fig. 2. Effect of mill scale concentration on MO decomposition. Experimental conditions: $[\text{MO}] = 0.1\text{mM}$; $\text{H}_2\text{O}_2 = 2\text{ ml}/100\text{ ml}$; reaction time = 60 min.

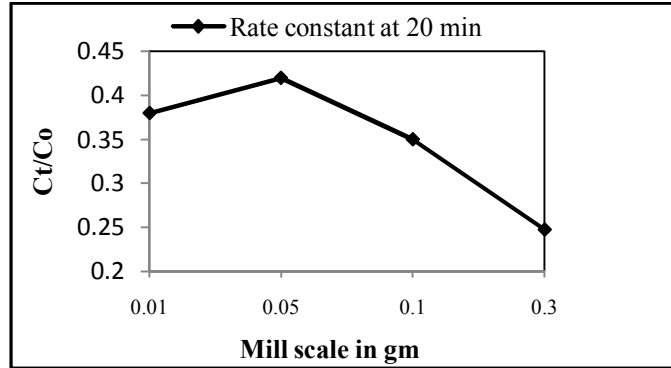
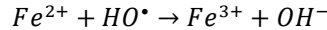


Fig. 3. Rate constant curve showing effect of mill scale concentration on MO decomposition. Experimental conditions: [MO] = 0.1 mM; H₂O₂ = 2 ml/100 ml; reaction time = 20 min.

Fe²⁺ also has a catalytic decomposition effect on H₂O₂. When Fe²⁺ concentration is increased, the catalytic effect also increases accordingly and when its concentration was higher, a great amount of Fe³⁺ was produced.



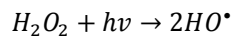
Moreover, Fe³⁺ ion could react with H₂O₂ to form hydroperoxyl radicals which is significantly less oxidizing agent than HO[•] [17].

In addition decomposition occurs in the suspension of mill scale in MO solution since mill scale is not soluble in water. So penetration of the UV light into the sample is highly dependent upon its concentration. At higher concentration, solution becomes opaque and light radiation cannot enter in to activate the catalyst particles. Hence the rate of dye degradation decreases [18].

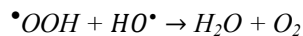
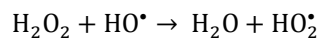
3.3. Effect of Hydrogen Peroxide concentration in MO decomposition

Another set of experiments were carried with varying the amount of H₂O₂ from 1 ml to 4 ml for 100 ml 0.1 mM MO decomposition. It was found (Figure 4) that the rate of decolorization rises by increasing the initial dosage of H₂O₂ up to a ‘critical’ value at which it is maximum and beyond which it is inhibited [19, 20, 21]. This phenomenon could be explained by considering the two opposing effects of H₂O₂ in the photo-oxidation reaction, explained as follows:

When increasing quantities of H₂O₂ are added to the solution, the fraction of light absorbed by the photo-decomposition increases, and, consequently, so does its photolysis rate. More hydroxyl radicals are available for dye oxidation [19, 22].



If additional H₂O₂ is used, excess H₂O₂ acts as a scavenger of highly reactive OH free radicals to form much less reactive peroxy radicals which further consume HO[•] forming oxygen. This can be expressed by the following reactions [22, 23, 24].



In addition, HO[•] radicals, generated at high local concentration, will readily dimerize to H₂O₂. As a consequence, there should be a favorable hydrogen peroxide concentration for the effective removal of dyes,

corresponding to the maximum color degradation, so an optimum hydrogen peroxide concentration exists. Thus if H_2O_2 concentration is increased above this limiting value, competition for HO^\bullet can be anticipated.

These predictions are in good agreement with the experimental data which is clearly observed from rate constant curve shown in figure 5. Here decomposition rate is the fastest for 2 ml H_2O_2

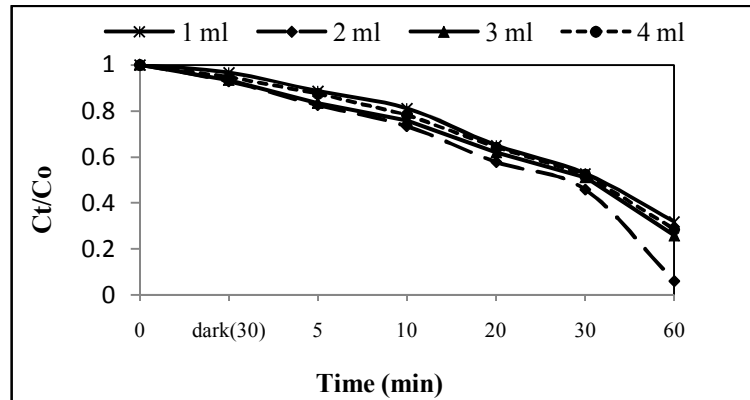


Fig. 4. Effect of H_2O_2 concentration on MO decomposition. Experimental conditions: $[\text{MO}] = 0.1 \text{ mM}$; Mill scale = 0.05 g/100 ml ; reaction time = 60 min

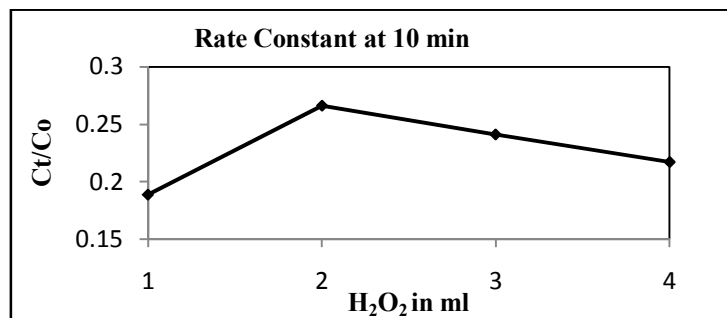


Fig. 5. Rate constant curve showing effect of H_2O_2 concentration on MO decomposition. Experimental conditions: $[\text{MO}] = 0.1 \text{ mM}$; Mill scale = 0.05 g/100 ml ; reaction time = 10 min

3.4. Effect of MO concentration on decomposition rate

A set of experiments were performed by varying MO concentration from 0.01 mM to 0.1 mM . Variation in MO concentration shows that lower the concentration higher the reaction rate although higher concentration can also be decomposed under UV (Figure 5).

An explanation to this behavior is that the higher the initial concentration, the higher the adsorbed organic substances on the surface of the catalyst and the solution became more intensely colored. Therefore, there are only fewer active sites for adsorption of OH^- so the generation of $\bullet\text{OH}$ will be reduced. Furthermore, as the concentration of methyl orange increases with constant intensity of UV illumination, the path length of photons entering the solution decreased, so only fewer photons reached the catalyst surface. As a result, the productions of holes or hydroxyl radicals that can attack the pollutants were limited. Therefore, the relative number of $\bullet\text{OH}$ attaching the compound decreases and thus the photodegradation efficiency decreases [25].

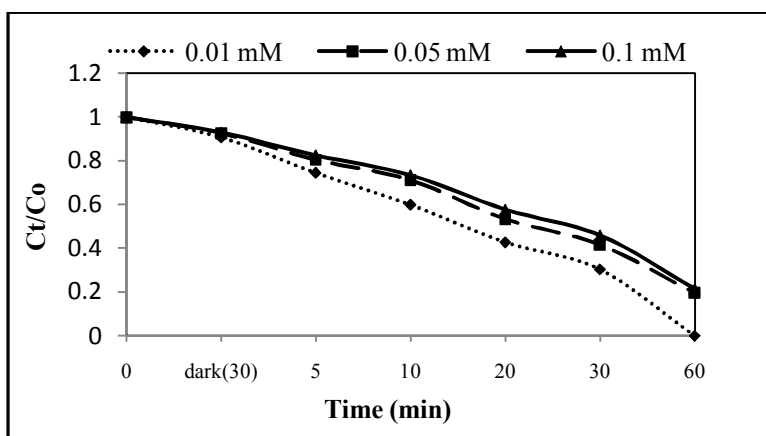


Fig 5: Effect of MO concentration variation on MO decomposition; Experimental conditions: Mill scale = 0.05 g/100 ml; H₂O₂ = 2 ml/100 ml reaction time = 60 min

4. Conclusion

Experimental results indicated that the combination of mill scale, hydrogen peroxide and light illumination is essential for the photodecomposition of MO. The rate of decolorization increased with an increase in mill scale & hydrogen peroxide upto an optimum value beyond which it decreased again. Moreover although any concentration of dye can be decomposed by using optimum amount of other catalysts but reaction rate increases with decreasing dye concentration.

Acknowledgements

The authors are grateful to Bangladesh University of Engineering and Technology (BUET) for providing facilities to carry out this research work.

Reference

- [1] D.L.Sedlak, A.W.Andren, Aqueous-phase oxidation of polychlorinated biphenyls by hydroxyl radicals, *Environ.Sci.Technol*, 1991, pp. 1419-1427.
- [2] E.Kusvuran, S.Irmak, H.I.Yavuz, A.Samil, O.Erbatur, Comparison of the treatment methods efficiency for decolorization and mineralization of Reactive Black 5 azo dye, *J.Hazard.Mater*, 2005, pp. 109-116.
- [3] G.V.Buxton, C.L. Greenstock, W.P.Helmen, A.B.Ross, Critical Review of rate constants for reactions of hydrated electrons *Chemical Kinetic Data Base for Combustion Chemistry. Part 3: Propane*, *J.PhysChem*, 1988, p. 513.
- [4] J Feng, X Hu, Yu e PL, Zhu HY, L u GQ. Discoloration and mineralization of Reactive Red HE-3B by heterogeneous photo-Fenton reaction. *Water Res*, 2003, pp. 3776-3384.
- [5] M.Pera-Titus, V.Garcia-Molina, M.A.Banos, J.Gimenez, S.Esplugas, Degradation of chlorophenols by means of advanced oxidation processes: a general review, *Appl. Catal*, 2004, pp. 219-256.
- [6] M.L.Kremer, Mechanism of the Fenton reaction. Evidence for a new intermediate, *Phys.Chem. Chem.Phys*, 1999, pp. 3595-3605.
- [7] PK Malik, SK Saha. Oxidation of direct dyes with hydrogen peroxide using ferrous ion catalyst. *SepPurifTechnol*, 2003, pp. 241-250.
- [8] S M K Nazrul Islam, ASW Kurny, F Gulshan, Photocatalytic Efficiency of Mill Scale for the Degradation of Textile Dye by Photo Fenton and Photo-Ferrioxalate System Under UV and Sunlight, *Environment and Ecology Research*, 2013, pp. 129-134.
- [9] Lucas, M. S. and Peres, J. A., "Decolorization of the azo dye Reactive Black 5 by Fenton and Photo-Fenton oxidation," *Dyes and Pigm*, 2006, pp. 236-244.
- [10] Huang, K. C., Couttenye, R. A., George, E. and Hoag, G. E., "Kinetics of heat-assisted persulfate oxidation of methyl tert-butyl ether (MTBE)," *Chemosphere*, 2002, pp. 413-420.

- [11] Sun, J. H., Sun, S. P., Wang, G. L. and Qiao, L. P., "Degradation of azo dye Amido black 10B in aqueous solution by Fenton oxidation process," *Dyes Pigm.*, 2007, pp. 647-652.
- [12] Garrido-Ramírez, E. G., Theng, B. K. G and Mora, M. L., "Clays and oxide minerals as catalysts and nanocatalysts in Fenton-like reactions — A review," *Appl. Clay Sci.*, 2010, pp. 182-192.
- [13] Barbusiński, K. and Majewski, J., "Discoloration of Azo Dye Acid Red 18 by Fenton Reagent in the Presence of Iron Powder," *J. Environ. Stud.*, 2003, pp. 151-155.
- [14] Cheninia, H., Djebbar, K., Zendaouib, S. M., Sehilia, T. and Zouchoune, B., "Removal of an Azo Dye (Orange G) By Various Methods in Homogenous Phase. Comparative Study," *Jordan J. Chem.*, 2011, pp. 307-319.
- [15] Tang, Z. W. and Chen, Z. R., "Decolorization kinetics and mechanisms of commercial dyes by H₂O₂/iron powder system," *Chemosphere*, 1996, pp. 947–958.
- [16] Benitez, F. J., Acero, J. L., Real, F. J., Rubio, F. J. and Leal, A.I., "The role of hydroxyl radicals for the decomposition of p-hydroxy phenylacetic acid in aqueous solutions," *Water Res.*, 2001, pp. 1338-1343.
- [17] Neyens, E. and Baeyens, J., "A review of classic Fenton's peroxidation as an advanced oxidation technique," *J. Hazard. Mater.*, 2003, pp. 33-50.
- [18] Sun, J., Qiao, L., Sun, S. and Wang, G., "Photocatalytic degradation of Orange G on nitrogen-doped TiO₂ catalysts under visible light and sunlight irradiation," *J. Hazard. Mater.*, 2008, pp. 312-319.
- [19] Sun, J. H., Sun, S. P., Sun, J. Y, Sun, R. X., Qiao, L. P., Guo, H.Q. and Fan, M. H., "Degradation of azo dye Acid black 1 using low concentration iron of Fenton process facilitated by ultrasonic irradiation," *Ultrason. Sonochem.*, 2007, pp. 761-766.
- [20] Sun, J. H., Shi, S. H., Lee, Y. F. and Sun, S. P., "Fenton oxidative decolorization of the azo dye Direct Blue 15 in aqueous solution," *Chem. Eng. J.*, 2009, pp. 680-683.
- [21] Wang, S., "A Comparative study of Fenton and Fenton-like reaction kinetics in decolourisation of wastewater," *Dyes Pigm.*, 2008, pp. 714-720.
- [22] Modirshahla, N., Behnajady, M. A. and Ghanbary, F., "Decolorization and mineralization of C.I. Acid Yellow 23 by Fenton and photo-Fenton processes," *Dyes Pigm.*, 2007, pp. 305-310.
- [23] Kang, N., Lee, D. S. and Yoon, J., "Kinetic modeling of Fenton oxidation of phenol and monochlorophenols", *Chemosphere*, 2002, pp. 915-924.
- [24] Bergendahl, J. A. and Thies, T. P., "Fenton's oxidation of MTBE with zero-valent iron," *Water Res.*, 2004, pp. 327-334.
- [25] R. M. Mohamed, I. A. Mkhallid, E. S. Baeissa, and M. A. Al-Rayyani "Photocatalytic Degradation of Methylene Blue by Fe/ZnO/SiO₂ Nanoparticles under Visiblelight." Hindawi Publishing Corporation, *Journal of Nanotechnology*, 2012, p 5.



6th BSME International Conference on Thermal Engineering (ICTE 2014)

A Study on Thermo-Catalytic Degradation for Production of Clean Transport Fuel and Reducing Plastic Wastes

M. A. Hazrat^{a,*}, M. G. Rasul^a, M. M. K. Khan^a

^a*School of Engineering & Technology, Central Queensland University
North Rockhampton, QLD 4702, Australia*

Abstract

Both the landfilling and incineration processes of plastic waste management system are identified as sources of pollutant gas emitters. Reprocessing is also uneconomical in comparison to the virgin plastic products in terms of commercial values due to polymeric contamination. This article studies the thermo-catalytic conversion processes waste plastics. The reaction conditions and the quantification of types of catalysts used for the conversion processes influenced the quality of the resultant hydrocarbons. Obtaining higher yield of conversion and transport grade fuel require more investigation to adapt this technical process as one of the effective alternative resources for fuel production. Thermo-catalytic process resolves the problem of halogen contents in the PVC type plastics by converting them into residues with the use of NaHCO₃ and AgNO₃ which capture chlorine type products from the gaseous hydrocarbons. Addition of catalysts in the convenient reactor reduces the requirement of higher temperature operations like thermal cracking processes and produces more liquefied products. It has been observed that, the aromatic plastic contents should be observed during the conversion process to obtain fuels based on allowable aromatic contents according to the fuel standards and emission regulations implemented in respective regions. The temperature of the process need to be controlled as per the boiling points of the mixture contents to avoid formation of vapor in the reactor which could causes sticky adherence to the reactor walls. A continuous liquid fractionating distillation process can reduce the formation of light gases in the yield. It was also found that the mixture of LDPE, HDPE, PP and PS yield 87.19% fuel with 20 wt% ZnO catalyst at 200 – 400 °C in a steel reactor. These fuels can be used directly in the automotive engines or can be retreated in the refineries to divide into gasoline and diesel fuels as per carbon chains. Since the plastic feedstocks do not contain any sulfur components the produced fuel can be treated as clean enough. Thus the fuels produced from this process can be considered as one of the potential alternative resources of fuel production resulting into an effective reduction of plastic wastes in a country.

© 2015 The Authors. Published by Elsevier Ltd.

Peer-review under responsibility of organizing committee of the 6th BSME International Conference on Thermal Engineering (ICTE 2014).

* Corresponding author. Tel.: +61749369634;
E-mail address: h.ali@cqu.edu.au

Keywords: plastic waste management; alternative fuel; pyrolysis; catalytic cracking; thermocatalytic cracking; incineration; plastic recycling

1. Introduction

Plastic wastes can be turned into a valuable alternative resource of energy production. True recycling of waste materials, i.e. converting the wastes into useful products to be reused effectively, can cut down the net cost of waste collection, sorting and reprocessing [1]. Statistically, the average worldwide consumption of various types of plastics is almost found as 35% high-density polyethylene (HDPE), 23% polypropylene (PP), 10% polystyrene (PS), 13% polyvinyl chloride (PVC), 7% poly-ethylene terephthalate (PET), and 12% miscellaneous polymers. Due to special practices of consumers, polyolefin (PE and PP) and PS are the most prevailing plastics in the waste polymers' stream [2].

Nomenclature

ABS	Acrylonitrile-butadiene-styrene
PE	Polyethylene
ZSM	Zeolite Socony Mobil

Since most of the plastic products are thrown out after single use it has been significantly contributing the accretion of plastic solid wastes in earth. There are social, economic as well as political aspects of waste disposal systems along with the key technical challenges associated to the appropriate and efficient disposals. This is the reason why several different methods have been explored and applied to resolve the issues related to the polymer waste handling and disposal. From the very beginning of waste disposal activities, landfills dumping of all types of biodegradable and non-biodegradable wastes as well as incineration of combustible wastes are considered the mostly adopted processes. Both the landfilling and incineration processes of plastic wastes cause a loss of the available alternative energy resources. There are lot of direct, indirect, short or long term pollutions observed for these activities. These types of disposal processes are no longer encouraged in order to protect the environment. Numerous investigations on both the environmental and economic effect of various recycling processes have been conducting around the world. Since plastics are produced from petrochemical substances they have significant calorific values. Most of the consumed plastics possess more calorific values than few of the mostly used fuels like coal and gas (Table 1). That means the waste plastics can be used to recover energy [3].

Table 1. Heat capacity comparison between various plastics and other materials [4, 5]

Plastic Material	Heat capacity (MJ/kg)	Other materials	Heat Capacity (MJ/kg) [* MJ/m ³ @0°C]
PVC	18	Heavy fuel oil	41
PP	46.4	Petrol/Gasoline	44
PE	47	Coal	26
PET	46	Natural gas	36*
PS	41	Milled peat	10
ABS	35	Paper	17

According to forecasts, the consumption of plastics is increasing at a rate of 4-5% annually [2]. The recycling rates as well as the energy recovery of plastic wastes have been increasing and it is still wasting a lot of potential resources for energy recovery in the modern world. In reality, it needs about 7 yards of landfilling space to dump 1 ton of plastic wastes in the land [3]. Also recycling of plastic products can save about 80% of energy required to make products like bottle, containers and other items. As the energy economy is a great concern, such a waste of energy cannot be overlooked. For that reason, recycling of plastic wastes in the form of clean energy production

could be certainly an effective option. Thus the waste management complexities can be resolved. Though it requires a lot of techno-economic implementation, it is not an unattainable option [6].

Despite the implementation of various policies like clean environment, developed technologies and waste reduction, it is not likely that the volumes of plastic wastes will decline. New recycling methods will have to be developed. From the perspective of catalysis, chemical recycling of plastic wastes is the most noteworthy of plastic waste recovery techniques [4]. Though mechanical recycling can lead to recovery of plastic wastes effectively, it is restricted to the thermoplastics, homogeneity of the types, contamination level and colour similarity [4, 5]. For plastic producer, the quality and the stability of the reprocessed product is a major obstacle [7]. Presence of hazardous additives and impurities in the mixed plastic waste stream limits the reprocessing efficiency. There is possibility of non-compliance with the food safety, medical instruments, and automobile equipment safety concern. Small amount of dissimilar resins can subjugate the commercial acceptance of the reprocessed plastics in compare to the virgin plastic made products. This recycling process cannot recover all the plastic wastes. The sorting of plastic wastes require more labour hours or sophisticated technological applications resulting increase of expenditure in the recovery process.

On the other hand, use of the plastic wastes as the source of feedstocks to produce fuels, monomers of the virgin plastics or various industrial chemicals have been considered as one of the most economic reprocessing options of waste management system. This process is also stated as tertiary or chemical recycling system. Based on the types of plastic wastes, various chemical or catalytic agents are used to obtain the desired products [5, 8]. Hydrogenation, gasification, chemical depolymerization, thermal treatments, catalytic cracking and reforming, etc. are considered as various types of feedstock based recycling process for plastic and rubber based wastes [5]. These recycling processes (i.e. both the mechanical and feedstock recycling) reduce the environmental pollution which could occur due to incineration and landfills [9]. Low temperature pyrolysis followed by a catalytic cracking, i.e. the continuous catalytic pyrolysis of HDPE gives more production of light olefins than the catalytic or pyrolysis process alone [10]. Similarly, Serrano et al. [11] investigated and found that two step processes could be adopted as one of the feasible technical processes to reduce waste plastics from the environment and produce transport grade fuels. In that case, among the various recycling methods of plastic wastes combination of the thermal cracking and catalytic cracking or the thermo-catalytic degradation are considered as commercially potential to obtain transport grade liquid fuels [11, 12]. There are still some techno-economic limitations for an efficient and complete recycling process development for waste plastics in terms of converting them into utile substances like liquid fuels.

This paper reviews the potential features of thermo-catalytic degradation of waste plastics as an alternative and effective way of waste reduction from environment. Also the potential of producing transport grade fuels following controlled process parameters of thermo-catalytic degradation has been reviewed. The usefulness of selective catalysts and their quantification, reaction temperature and the time to degrade the polymer into optimal liquid fuel yield has been discussed in brevity. It is expected that this potential technical process can be effectively utilized for commercial production of transport grade fuel and consequently plastic waste management system will be implemented in desired way.

2. Plastic waste management

Generally if the recycling is performed with the plastic products collected from the waste stream, they are not reused to produce the same product due to quality concerns [13]. Due to low grade utilization of the recycled plastic materials, alternative recycling processes are evaluated and further improvement is going on. Several preliminary issues have been discussed in this section so that the importance of the thermo-catalytic process can be perceived well.

2.1. Plastic wastes in Australia and USA

In case of Australia, the recycling rate of plastic wastes was 20.8% in the year 2012-2013 [14]. Out of total plastic consumption of 1.477 million tons, 307,300 tons were recycled (145,600 tons domestically and 161,800 tons sent to overseas). In USA, there were about 39.3 million tons of waste plastics generated in 2011[15]. It was nearly 11% of

the total municipal solid waste stream for that year. Of this total plastic wastes, 2.66 million tons (6.8%) were recycled, 3.9 million tons (9.9%) were converted to energy in waste-to-energy (WTE) plants, 0.27 million tons (0.7%) were used as alternative fuel in cement production, and the rest 32.5 million tons (82.7%) were dumped for landfills. Also, there were about 1.9 million tons of non-recyclable plastic wastes generated in the form of automotive shredder residue (ASR) [15]. Along with USA, Japan and Western Europe are also producing lot of waste plastics. China and India are also producing more and more waste plastics rapidly [16, 17]. Fig. 1 (adopted from [18]) represents the alarming track of plastic waste increment worldwide. Thus, plastic waste management and environment protection are key issues in everywhere in this world.

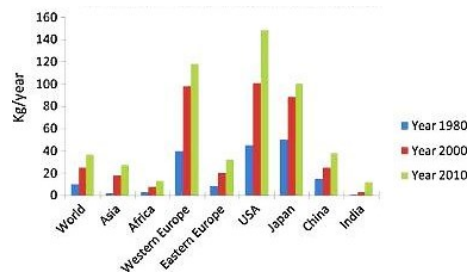


Fig.1. Regional per capita plastic consumption data (kg/year) [17]

2.2. Landfilling of plastic wastes

Waste plastics are not biodegradable; they remain for long period into the landfill. The lack of landfill sites and assessments of the environmental consequences of landfilling have led many countries to ban landfilling of combustible wastes, including wet organic waste [19, 20].

Landfilling of plastic wastes causes pollution by emitting toxic gases like furanes and dioxins to the environment which are carcinogenic. Various types of additives, i.e. fillers, plasticizers, colorants are used with virgin plastics to make them user friendly, hygienic, durable, UV resistant and economic for the consumers. Hence, plastics can pollute the environment due to presence of various additives. Mostly Nonylphenols, Polybrominated diphenyl ethers (PBDEs), di-(2-ethylhexyl) phthalate (DEHP), and Bisphenol A (BPA), are mixed with the monomers of virgin plastics to act as catalyst in producing polymers and thus enhance other desired properties. Some of these used chemicals are found responsible as hormone-disrupters [21]. Bisphenol A (BPA), which is extensively used with the epoxy resins of food and beverage containers and as monomer in the polycarbonate plastic of many consumer products, is alarmingly related to cardiac diseases, diabetes as well as abnormal increase of certain liver enzymes [22]. PBDEs may be responsible for lowering the immune system, thyroid disruptions, and troubles in fertility issues of human being. So, when plastics are used or discarded, the emissions based on these additives are undesirable from an environmental point of view [23]. The American Chemistry Council (ACC) reported that if all of the landfilled municipal solid wastes in USA could be diverted into waste to energy production processes it could reduce the coal consumption by 108 million tons. This is equivalent to the production of 162 million MWh of electricity for 16.2 Million households for one year [24]. Even the biodegradable plastics are liable for methane based greenhouse gas emission to the environment. Leachate forming is also another threat that can pollute the ground water being soaked by the soil.

2.3. Incineration of plastic wastes

On the other hand, incineration of wastes has been considered as the highly effective method to reduce the volume of wastes by producing energy. In most countries, it is the traditionally adopted technology. So, there is a widespread concern about the methodologies regarding incineration process and the emissions related to it. Air pollutants like CO, CO₂, NO_x, SO_x, particulate matters (PM), volatile organic compounds (VOCs), and polycyclic aromatic hydrocarbons (PAHs) are found from the plastic waste incinerations [23, 25]. Almost 30% by weight of waste plastics are converted into CO₂ due to this process with a factor of 25 gm/MJ fuel to be compared with other

fuels [26]. Though the incineration process converts the waste into energy for industrial uses in some extent, the conversion efficiency and the emitted pollutants are endangerment concerns. Plastic wastes are generally burnt for few seconds in high temperature (e.g. 2 sec, 850 OC or higher) incinerators with an excess air ratio between 1.0 and 1.8 [25, 27]. The ash by-products of incineration process are generally landfilled and are of risk based concerns due their carcinogenic threat [24]. Enforcement of new legislations, increased expense, social as well as ecological awareness, stringent strategies of environment protection, etc. are the restricting factors to the disposals of both organic as well as plastic wastes in the landfills and incinerators [28].

3. Thermo-catalytic degradation of plastic wastes

There is a significant difference between thermal and catalytic cracking processes – in terms of reaction condition, raw material feeding system and product output. Thermal cracking can be explained by a free radical mechanism [29] and the catalytic cracking can be recognized by carbonium ions [30] consisting of single positive charge carrier ions from the hydrocarbon. The controlled combination of these two processes helped reducing the process operation costs and increased the conversion efficiency along with the desired products [10-12, 28].

3.1. Thermal cracking (pyrolysis and liquefaction)

In the thermal cracking/pyrolysis process, the reaction is performed within the temperature region of 350-800 OC and the plastic materials are degraded in absence of both air/oxygen and catalysts [17]. The type of plastics or the mixture proportion of various plastic polymers governs the performance of the pyrolysis process along with the other parameters like temperature, reactors, residence time and product removal systems, heating rate, operating pressure, etc. [31]. The lighter molecular weight/less dense polymers require higher temperature in the pyrolysis process resulting in a wide range of hydrocarbons. Gases, light oils and chars are the main products of the process based on the governing parameters, which need further treatment (Condensation, Hydrotreating, Hydrocracking, Distillation, etc.) to convert into transport grade fuels. Typical pyrolysis features some drawbacks. Cooking of the reactor walls, sticking of plastics in the reactor walls are undoubtedly experienced in this process. As a result, the heat transfer efficiency is reduced resulting of fewer yields of liquid products (known as bio-oil). Periodic cleaning of the reactor becomes essential in such cases. Stirring of the molten polymers in the reactor as well as continuous removal of those molten polymers can resolve these obstacles in a large extent.

The thermal cracking process in presence of N₂ gas pressure system is termed as pyrolysis, whereas the similar reaction under H₂ gas pressure system is known as liquefaction [32]. Williams & Edward [32] conducted thermal cracking on various plastics under the experimental condition of 500^oC (@5^oC/min), type T316 stainless steel made bench top reactor of maximum pressure capacity 19.2 Mpa , 1 hour, 0.2-10Mpa of N₂ gas (for pyrolysis), 1 Mpa of H₂ gas (for liquefaction), etc. for the following observations (Table 2). This table infers that the liquefaction process yields less aromatic contents and produces more liquid substances. Hence the further treatment of producing the transport grade fuel from thermal cracking may be conducted with the liquefaction process if process expenditure is comparable. Also Zadogonkar & Umesh [33] described that the pyrolysis of PVC may emit toxic substances like polychlorinated dibenzodioxins (PCDD), polychlorinated dibenzofurans (PCDF), polychloro biphenyls (PCB) along the hydrochloric acid, which is corrosive. Both the higher amount of residues and the liquids of pyrolysis process have lower octane rating to be processed as transport grade fuel [17].

Baker [34] pointed out few issues about pyrolysis process of converting plastic wastes into fuel, which are: frequency of reactor chamber cleaning requirement is very high; poor heat conductivity within plastics; processing time increases with load in the chamber; high expenditure of consumable catalysts due to fouling; produced fuels lack tolerance to be suitably used in the engines or industrial machines instead of fossil fuels; flash point of the produced fuels are lower than that of diesel (45°C ~ 53°C) and usually vary in wide ranges (25°C ~ 45°C) due to presence of light hydrocarbons; and to perform as diesel fuel, the inventors have found that the fuel must be substantially rich in chains with a carbon chain length peaking around C16 (i.e. cetane). But removal of lighter fraction hydrocarbon contents (5-7% wt) of boiling point lower than 160°C from the pyrolysis process outputs can lead to the improvement of flash point the fuel.

Table 2. Product yields of different thermal cracking processes

Plastic	Oil (wt%)	Gas (wt%)	Residue (wt%)	Total aromatic and PAH compounds (wt%)	Pyrolysis Process			
					Oil (wt%)	Gas (wt%)	Residue (wt%)	Total aromatic and PAH compounds (wt%)
					Liquefaction Process			
PE	93	7	0	16.4	95	5	0	15.5
PP	95	5	0	18.8	95	5	0	17.1
PS	71	2	27	100.0	77	2	22	100.0
PVC	-	-	-	-	2	38	52	52.7
PET	15	32	53	32.7	27	32	41	22.0
Waste DSD (mixed)	32.5	0.5	50.2	29.6	48.2	2.2	35.1	24.1
Waste Fost Plus (mixed)	64.1	4.3	23.3	27.6	70.6	4.9	17.8	24.9

Generally, the pyrolysis process operating on higher temperatures yields more gaseous and residues. The optimal working temperature zone of producing diesel or gasoline type liquid products is about 390–425 OC. Due to higher operating temperature, the composition of the yield products also changes into aromatic dominant than those of aliphatic compounds found in lower temperature [35, 36]. Both the residence time and the temperature of pyrolysis process control the quality of the yield product. Since the pyrolysis yields cannot be directly used as transport fuels, further improvement has been essential.

3.2. Catalytic and thermo-catalytic cracking

Catalysts help reducing the activation energy of the feedstock so that the required temperature in the thermal cracking process is reduced and the reaction rate is increased. Also the yield products are within the narrow range of hydrocarbons [37]. For instance, with various concentrations of SO₃ catalysts in the catalytic pyrolysis reaction of HDPE, the activation energies of HDPE, HDPE+3.5%SO₃ and HDPE+7%SO₃ are 342.95, 159.96, 132.61 KJmol⁻¹ respectively [38]. The boiling point of the gasoline, diesel, heavy oils and waxes ranges from 50-220 OC, 220-340 OC, 340-420 OC, 420-480 OC respectively. But the volatility of the compounds obtained from pyrolysis of various waste plastic products range widely. To obtain clean and stabilized petroleum fuel, the pyrolytic syngas and oils are treated in further stages [18]. Silica-alumina and the zeolites are mostly used to change both the volatility and nature of product of the pyrolytic oils [39]. Also the reactive acidic components of the pyrolytic oils can be eliminated by using Na-zeolite or aluminated MCM-41 catalysts. The Na-zeolites can effectively perform the de-halogenation of pyrolytic oils obtained from the halogenated plastics or electronic wastes [39]. With increasing number of acid sites, the level of the catalyst activity in polyolefin pyrolysis also increases. Zeolite-based catalysts due to their high acid strength achieve higher conversion than nonzeolitic catalysts [9].

Catalysts can be introduced into the reactors by either mixing the liquid form with the plastics before reaction occurs or mixing as vapor in the volatile fraction stream of pyrolysis or gasification processes [17]. Either of the processes is effective in terms of liquid yield. The ratio between catalyst and the polymer waste also controls the liquid fuel conversion efficiency of the process. Though several research outputs have shown that the increase of catalyst content increases the amount of desired fuel like liquid products, there is an optimal range. The conversion efficiency even decreases after the optimal range of catalyst to waste plastic ratio based on the type of catalysts, plastics, and reaction temperature [12]. Acidity of the catalysts governs the quantity of the desired liquid yield. Highly acidic active catalysts can lead to further cracking of the liquid hydrocarbon in the reaction chamber resulting into more gaseous products and coke [12].

Generally the cracking of HDPE produces more linear n-paraffins. But the presence of linear paraffins in diesel fuel causes gelled suspension in normal temperature. As a result, it requires isomerization to produce branched isomers so that both the cloud point and the freezing point of the fuel can be lowered with the reduction of formation

of wax crystals [40]. Catalytic dewaxing [36] of the yield fuels can be considered one of the effective methods to overcome these issues along with lowering the boiling range (T95). This process also retains the cetane rating of the diesel fuel derived from plastics. The catalysts are preferably of large pore sizes and higher silica (e.g, Beta-zeolite/high silica Y) based or ZSM-5, ZSM-11, ZSM-12, ZSM-22, ZSM-23, ZSM-35 and ZSM-38 for dewaxing isomerization. On the other hand, selective paraffin isomerization dewaxing [1] can be implemented with the catalysts like aluminosilicate zeolite to improve the fuel quality by handling only the linear n-paraffin. Thus the available highly branched-isomers, aromatic and cycloaliphatic compounds in the derived fuel are not affected by the catalyst.

Many studies on catalytic conversion of different types of plastic polymers to different products including chemicals and fuels, using different type of catalysts have been published [41]. The most widely used are Zeolite base catalysts such as ZSM-5 [42], silica, alumina [43], basic catalysts, such as BaCO₃ [44], Bimetallic catalyst Al-Zn composite [45], and FCC catalyst [46]. Despite the fact that most of these catalysts worked in terms of plastic waste conversion, still they are associated with either high cost of production or the operating condition may not be industrially feasible as high temperature and more residence time with low percentage conversion might be the case. Highly acidic behavior of the catalysts reduces the liquid yields but lighter hydrocarbons of gasoline categories [47]. Table 3 presents several more thermo-catalytic degradation processes and their yield compositions. It has been shown that the problem occurred in the pyrolysis process only with the PVC, PS and mixed plastics can be resolved by using appropriate solvent/light gas cleaner, e. g. NaHCO₃ + AgNO₃ mixed solution in a some appropriate quantity. The conversion rate of fuel standard liquid has been observed more than 50 wt% consisting of carbon chain length C3-C32.

Researchers [5, 35, 48, and 49] reported that the content of aromatic hydrocarbons may be small or even very small for non-catalyzed pyrolysis but in the presence of catalysts (particularly zeolites) they observed an increase in the amount of aromatic hydrocarbons in the liquid. Strongly acidic catalysts like HZSM-5 zeolites yield lighter hydrocarbons (C3-C6), whereas, the less acidic catalysts like microporous HMCM-41 can produce heavier hydrocarbons from conversion of waste plastics [36]. Manos et al. [37] observed that the order of catalysts' activity on HDPE could be presented as, (lighter hydrocarbons) ZSM-5 < mordenite < β < Y < US-Y (heavier hydrocarbons) and (alkenes dominant) ZSM-5 < mordenite < β < Y < US-Y (alkanes dominant). Choosing an appropriate catalyst for the particular plastic to obtain transport fuel is a key factor to successful accomplishment of the process.

Though, catalysts may decrease the temperature of the process, change the selectivity and the composition of the products, they give more gas product, the catalysts are quickly deactivated and recovering and regeneration of them is not easy. It may increase the costs of the process. Many researchers and inventors have proposed fluidized-bed reactors due to their advantages, i.e. difficulties with the mixing of the wastes, removing of the coke, regeneration of the catalyst, and heat transfer resistance may be solved and/or reduced in an easy way. However, the fluidized-bed reactors may be profitable probably only in large industrial-scale plants due to the investment costs [56].

The catalytic process followed by the thermal liquefaction of plastics with various catalysts can reduce the problems associated with the disintegration of the plastic wastes, wall to plastic particle heat transfer issues, sticking of the cracking raw materials with the reactor walls, cooking of reactor walls, etc. which are found in the thermal conversions only [56].

Table 3. Waste plastic to fuel conversion processes in presence of various catalysts

Type of Mixture	Plastic	Process	Temperature	Pressure	Catalysts	Time (min)	Solvent/light gas cleaner	% Fuel Yield	Remarks
Mixed Plastic [50]	50 gm PS + 25 gm PVC	Thermo-catalytic degradation (TCD)	200-430 °C		5 wt% ZnO	201	0.5(N) NaHCO ₃ + 0.2 (N) AgNO ₃	50.08% (C3-C32) (0.86gm/ml)	Cl content is high in PVC that is left as residue. Electricity Consumption 0.433KWh

Mixed Plastic [51]	50% waste plastics (LDPE, HDPE, PP, PS mixture) + 50% tire	Thermo-catalytic degradation (TCD)	250 - 430 °C		2 wt% $\text{Fe}_2(\text{CO}_3)_3$	270	0.5(N) NaOH + 0.25(N) NaHCO_3 + 0.25(N) AgNO_3	47.4% (C3-C20) (0.78 gm/ml)	Higher residue (37.7%) due to other contents in tire and PS that cannot be converted into fuel. Electricity Consumption 0.711 KWh
Mixed Plastic [52]	LDPE, HDPE, PP, PS mixture	Thermo-catalytic degradation (TCD)	200 - 400 °C		20 wt% ZnO	258	0.25(N) NaHCO_3 + 0.25(N) AgNO_3	87.19% (C3-C36) (0.77 gm/ml)	Plastics were cut into pieces of 2-3mm size. Electricity Consumption 6.25 KWh
[38] Homogeneous	HDPE	Catalytic degradation	400 °C (Heating rate of approximately 20°Cmin^{-1})		CAT1 (7% SO_3) and CAT2 (3.5% SO_3) modified Zirconium catalysts (Calcined @ 550°C for 3hrs then cooled down in desiccator before using.)			34.31% oil + 65.68% gas (with CAT1), and 53% oil + 46.98% gas (with CAT2)	Fixed-bed reactor. The sizes of the plastic and catalysts were 125-150 μ and 75-100 μ respectively. Oil composition with CAT1 is more of aromatic type which is favorable with gasoline. The oil yielded by CAT2 is olifinic (65%) which is good for industrial uses.
[1] Homogeneous	LDPE	Catalytic Pyrolysis	175-400 °C	Atm. Pressure	1g (20 wt%) CaC_2	60		69.73% fuel oil + 30.07% gas + 0.2%char	Batch reactor, Optimal liquid yield was found at 350 °C
Mixed Plastic [53]	24 wt.% HDPE + 39 wt.% LDPE + 21.5 wt.% IPP + 10 wt.% PS + 4 wt.% ABS + 1.5 wt.% PET	Thermo-catalytic decomposition	420-440 °C (For HZSM-5), and 450-480 °C (For PZSM-5),	Atm. Pressure	HZSM-5 and orthophosphoric acid modified (PZSM-5) zeolite catalysts	120		52 wt% liquid (with HZSM-5), and 47.33 wt% liquid (with PZSM-5)	Extruder type fixed bed reactor. Thermocatalytic process produces lighter olefins and paraffins along with increased alkyl aromatics.
[54] Mixed Plastic	PS and HDPE	catalytic degradation	400 °C (heating rate 9°C/min)	Atm. Pressure, N_2 stream (20 cc/min)	Catalyst: Reactant (1:10). Spent FCC catalyst.	38, 49			Semi-batch reactor (stirring speed of 200 rpm).

[16] Homogeneous	Waste Polypropylene	Catalytic pyrolysis	400 °C to 550 °C (10°C/min)	Kaolin clay (SiO ₂ 43.12%, Al ₂ O ₃ 46.07%, Fe ₂ O ₃ nil, MgO 0.027%, CaO 0.030%, ZnO 0.0064%, K ₂ O 0.01%, TiO ₂ 0.74) catalyst to plastics ratio (1:2, 1:3, 1:4, 1:6, 1:10, 1:20, 1:40)	87.5 wt% liquid (745 kg/m ³ , 2.18 Cst) + 11.75 wt% gaseous + 0.75 wt% residue	The highest yield of oil (87.5 wt%) was obtained at the ratio of plastics to catalyst 3:1 at 500°C. The catalysts could be reused for several times and reduces the activity after 4 times of re-using due to deposition of carbon and wastes over the catalyst's surface.	
[55] Homogeneous	LLDPE	catalytic degradation		20% and 40% ultrastable Y zeolite (US-Y)	N ₂ gas (50 ml/min) in order to remove the volatile yields	Semi-batch Pyrex reactor. containing only a small amount of zeolite, cracking catalysts are less acidic and produce, therefore, more liquid hydrocarbons than their parent zeolite	
[28]	HDPE	Catalytic cracking	381 °C - 427 °C	Al ₂ O ₃ (HDPE:Catalyst = 7:1)	N ₂ gas	Conversion efficiency 65.4% (89.6% liquid + 10.4% wax).	Semi-batch reactor with about 50% efficient electric heating system.
[56]	Polyolefins (HDPE, PP)	The melting and cracking process (<i>Clementi Process</i>) in tubular reactor with the molten metal bed called "the tube in the tube"	419 °C – 428 °C	Alloy based molten metal bed (59-61 wt% of Tin + 38-4 wt% of Lead + 1wt% of Impurities) of 8.5 g/cm ³ and melting temperature of 183-185 °C	93.31 wt% liquid (~10 mol% light wax, and ~50 wt% light gasoline) + 6.69 wt% gaseous hydrocarbons	No solid residue was found at the end of the conversion process. Products can be treated to produce transport grade fuel or directly used in electricity generation. The content of aromatic	

							hydrocarbons in liquid yield is lower than other reactors.
[57]	LDPE film	Catalytic Pyrolysis	550 °C (10 °C min ⁻¹)	NiMo/Al ₂ O ₃ (2.72 wt% Ni + 13.16 wt% Mo + 84.12 wt% Al ₂ O ₃). Plastic to catalyst ratio = 20:1	The reactor was completely purged with dry nitrogen to remove air.	Conversion efficiency is 93.8%. (85.3 wt% liquid + 8.5 wt% gaseous + 6.2 wt% solid residue), liquid fraction's heating value is 10,810 Cal/g, which is higher than that of fuel oil.	Batch reactor. Though the pyrolysis occurs in absence of oxygen, the presence of catalyst reduces the degradation temperature and increases the fraction of liquid yield.

4. Discussion

Every nation in the world, especially the highly populated as well as the developed countries, has been facing the continuous accretion of the plastic wastes in the garbage dumping places. Also, both the landfilling and incineration based waste dumping have been pushing the earth toward the environment saving challenges. Various types of diseases are now observed due to environmental pollution caused by these polymer wastes.

Pyrolysis (thermal cracking) process of waste plastics alone has been facing few obstacles to produce fuels according to the fuel standards. Thermal liquefaction in presence of hydrogen gas pressure system can produce more liquefied hydrocarbons than the nitrogen based thermal cracking system.

The catalytic cracking followed by the thermal liquefaction can facilitate the effective conversion of waste plastics into liquid fuel. Only catalytic process faces the obstacles with mixed and dirty plastics as the catalysts are mixed before the degradation starts. That causes production of more chars and wide ranges of hydrocarbons. But when the waste plastics are liquefied in presence of hydrogen and then the catalysts are introduced in the yield of this process, the combined process provides better process efficiency. Also the consumption of catalysts is optimized with this mixed mechanism. Moreover, the problem with the mixed plastics is resolved in this thermo-catalytic process.

Thermo-catalytic process can reduce the process temperature of the thermal cracking process alone. The liquefied and the gaseous hydrocarbons from the liquefaction process can be easily mixed with the catalysts. Therefore, the less catalyst consumption reduces the process expenditure. Besides, the problem with the PVC, PS type plastics can be resolved in the thermo-catalytic process with an optimal solution of NaOH, NaHCO₃, and AgNO₃. As a result, most of the unprocessed waste plastics can be fed into the thermal liquefaction chamber for fuel production purpose.

5. Conclusion

Various types of catalysts have been found effective in converting the plastics into desired fuel category products. Among them the Kaolin clay (SiO₂ 43.12%, Al₂O₃ 46.07%, Fe₂O₃ nil, MgO 0.027%, CaO 0.030%, Zn), Silica-Alumina, Zeolites (beta, USY, ZSM-5, REY, clinoptilolite, etc.), and MCM-41, etc. are the frequently used catalysts. In case of de-chlorination purposes, some light gas cleaners are used in optimal amount based on the plastic feedstock. The aromatic content and the corrosive contents are reduced due to this process. The integration of thermal liquefaction along with the catalytic process, the overall process temperature is reduced. The amount of desired transport grade fuel products increases. Also the use of environment friendly fuel in the vehicles can be

potentially increased. Use of waste plastics with such objectives can reduce the bulk increment of wastes in the environment. So, the thermo-catalytic process can be industrially or nationally sponsored to reduce solid polymer wastes from environment. Alternative fuel production can effectively reduce the fuel import load of any nation producing more plastic wastes.

Acknowledgements

Acknowledgements and Reference heading should be left justified, bold, with the first letter capitalized but have no numbers. Text below continues as normal.

References

- [1] Mabood F, Shah J, Jan MR, Hussain Z, Jabeen F. Catalytic Conversion of Waste Low Density Polyethelene into Valuable Products. *Journal of the Chemical Society*. 2010;32:574-81.
- [2] Tukker A, de Groot H, Simons L, Wiegiersma S. *Chemical Recycling of Plastics Waste (PVC and other resins)*. The Netherlands: TNO Institute of Strategy, Technology and Policy; 1999. p. 1-132.
- [3] Recycling C. *Plastic Recycling Facts. Complete Recycling*; 2014.
- [4] Ylä-Mella J. *Recycling of Plolymers*. 480360S *Environmental Catalysis*. Finland: University of Oulu; 2005. p. 1-9.
- [5] Aguado J, Serrano D. *Feedstock Recycling of Plastic Wastes*. UK: The Royal Society of Chemistry; 1999.
- [6] Le Guern Lytle C. *When The Mermaids Cry: The Great Plastic Tide*. USA: Santa Aguila Foundation; 2009.
- [7] Neidel TL, Jakobsen JB. *Report on initial assessment of relevant recycling technologies*. COWI A/S; 2013.
- [8] Janssen FJJG, Santen RAvRA. *Environmental catalysis*. London: Imperial College Press; 1999.
- [9] Cleetus C, Thomas S, Varghese S. *Synthesis of Petroleum-Based Fuel from Waste Plastics and Performance Analysis in a CI Engine*. *Journal of Energy*. 2013;2013:10.
- [10] Artetxe M, Lopez G, Amutio M, Elordi G, Bilbao J, Olazar M. *Light olefins from HDPE cracking in a two-step thermal and catalytic process*. *Chemical Engineering Journal*. 2012;207–208:27-34.
- [11] Serrano DP, Aguado J, Escola JM. *Developing Advanced Catalysts for the Conversion of Polyolefinic Waste Plastics into Fuels and Chemicals*. *ACS Catalysis*. 2012;2:1924-41.
- [12] Akpanudoh NS, Gobin K, Manos G. *Catalytic degradation of plastic waste to liquid fuel over commercial cracking catalysts: Effect of polymer to catalyst ratio/acidity content*. *Journal of Molecular Catalysis A: Chemical*. 2005;235:67-73.
- [13] Williams PT. *Waste Recycling. Waste Treatment and Disposal*: John Wiley & Sons, Ltd; 2005. p. 127-70.
- [14] A'Vard D, Allan P. 2012–13 *National Plastics Recycling Survey*. In: O'Farrell K, editor. Australia: Sustainable Resource Use Pty Ltd (ABN 52 151 861 602); 2012. p. 1-64.
- [15] Themelis NJ, Mussche C. 2014 *Energy and Economic Value of Municipal Solid Waste (MSW), Including Non-Recycled Plastics (NRP), Currently Landfilled in the Fifty States*. USA: Earth Engineering Center; 2014. p. 1-40.
- [16] Panda AK, Singh RK. *Experimental Optimization of Process for the Thermo-catalytic Degradation of Waste Polypropylene to Liquid Fuel*. *Advances in Energy Engineering (AEE)*. 2013;1:74-84.
- [17] Panda AK, Singh RK, Mishra DK. *Thermolysis of waste plastics to liquid fuel: A suitable method for plastic waste management and manufacture of value added products—A world prospective*. *Renewable and Sustainable Energy Reviews*. 2010;14:233-48.
- [18] Blazsó M. *Pyrolysis Oils of Plastic Wastes*. In: Müller-Hagedorn M, Bockhorn H, editors. *Feedstock Recycling of Plastics, Selected papers presented at the Third International Symposium on Feedstock Recycling of Plastics*. Germany: Universitätsverlag Karlsruhe 2005. p. 11-8.
- [19] Sarker M, Rashid MM. *Alternative Liquid Hydrocarbon Fuel Production: Comparative Study for Polypropylene Waste Plastic and Standard Plastic: Energy and Power*; 2013.
- [20] Maria FD, Pavesi G. *RDF to energy plant for a central Italian region SUW management system: Energetic and economical analysis*. *Applied Thermal Engineering*. 2006;26:1291-300.
- [21] Halden RU. *Plastics and Health Risks*. *Annual Review of Public Health*. 2010;31:179-94.
- [22] Lang IA, Galloway TS, Scarlett A, et al. *Association of urinary bisphenol a concentration with medical disorders and laboratory abnormalities in adults*. *JAMA*. 2008;300:1303-10.
- [23] Siddiqui MN, Redhwi HH. *Catalytic coprocessing of waste plastics and petroleum residue into liquid fuel oils*. *Journal of Analytical and Applied Pyrolysis*. 2009;86:141-7.
- [24] World WM. *Landfilled Plastics Could Power 5.2 Million U.S. Households*. *Waste to Energy: Waste Management World*; 2011.
- [25] Li C-T, Zhuang H-K, Hsieh L-T, Lee W-J, Tsao M-C. *PAH emission from the incineration of three plastic wastes*. *Environment International*. 2001;27:61-7.
- [26] Sundberg J, Olofsson M. *Waste-to-Energy Incineration*. Gothenburg, Sweden: Profu consultancy firm; 2004. p. 1-36.
- [27] Lea WR. *Plastic incineration versus recycling: a comparison of energy and landfill cost savings*. *Journal of Hazardous Materials*. 1996;47:295-302.
- [28] Stelmachowski M, Słowiński K. *Thermal and thermo-catalytic conversion of waste polyolefins to fuel-like mixture of hydrocarbons*. *Chemical and Process Engineering*. 2012;33:185-98.

- [29] Cullis CF, Hirschler MM. The combustion of organic polymers. The University of Michigan, USA: Clarendon Press; 1981.
- [30] Buekens AG, Huang H. Catalytic plastics cracking for recovery of gasoline-range hydrocarbons from municipal plastic wastes. *Resources, Conservation and Recycling*. 1998;23:163-81.
- [31] Gao F. *Pyrolysis of Waste Plastics into Fuels*: University of Canterbury; 2010.
- [32] Williams PT, Slaney E. Analysis of products from the pyrolysis and liquefaction of single plastics and waste plastic mixtures. *Resources, Conservation and Recycling*. 2007;51:754-69.
- [33] Zadaonkar, Umesh. A catalyst composition for catalytic cracking of waste plastic. In: Organization WIP, editor. India2005. p. 1-20.
- [34] Baker G. Process for conversion of waste material to liquid fuel. Google Patents; 2005.
- [35] Bennett GF. Feedstock Recycling and Pyrolysis of Waste Plastics, J. Scheirs, W. Kaminsky (Eds.). John Wiley & Sons Ltd., Chichester, West Sussex, England (2006), ISBN: 0-470-02152-7. *Journal of Hazardous Materials*. 2007;147:682-3.
- [36] Scheirs J. Overview of Commercial Pyrolysis Processes for Waste Plastics. In: Scheirs J, Kaminsky W, editors. *Feedstock Recycling and Pyrolysis of Waste Plastics: Converting Waste Plastics into Diesel and Other Fuels*. Chichester, West Sussex, England: John Wiley & Sons Ltd.; 2006. p. 383-433.
- [37] Manos G, Garforth A, Dwyer J. Catalytic Degradation of High-Density Polyethylene over Different Zeolitic Structures. *Industrial & Engineering Chemistry Research*. 2000;39:1198-202.
- [38] Almustapha MN, Andresen JM. Catalytic Conversion of High Density Polyethylene (HDPE) Polymer as a means of recovering valuable energy content from the plastic wastes International Conference on Petroleum and Sustainable Development Singapore: IACSIT Press; 2011. p. 21-6.
- [39] Uemichi Y, Nakamura J, Itoh T, Sugioka M, Garforth AA, Dwyer J. Conversion of polyethylene into gasoline-range fuels by two-stage catalytic degradation using silica-alumina and HZSM-5 zeolite. *Industrial Engineering Chemistry Research*. 1999;38:385-90.
- [40] Ali S, Garforth AA, Harris DH, Rawlence DJ, Uemichi Y. Polymer waste recycling over “used” catalysts. *Catalysis Today*. 2002;75:247-55.
- [41] Lin Y-H. Production of valuable hydrocarbons by catalytic degradation of a mixture of post-consumer plastic waste in a fluidized-bed reactor. *Polymer Degradation and Stability*. 2009;94:1924-31.
- [42] Park DW, Hwang EY, Kim JR, Choi JK, Kim YA, Woo HC. Catalytic degradation of polyethylene over solid acid catalysts. *Polymer Degradation and Stability*. 1999;65:193-8.
- [43] Lin Y-H, Sharratt PN. Catalytic Conversion of Polyolefins to Chemicals and Fuels over Various Cracking Catalysts. *Energy & Fuels*. 1998;12:767-74.
- [44] Shah J, Jan MR, Mabood F, Jabeen F. Catalytic pyrolysis of LDPE leads to valuable resource recovery and reduction of waste problems. *Energy Conversion and Management*. 2010;51:2791-801.
- [45] Tang C, Wang Y-Z, Zhou Q, Zheng L. Catalytic effect of Al-Zn composite catalyst on the degradation of PVC-containing polymer mixtures into pyrolysis oil. *Polymer Degradation and Stability*. 2003;81:89-94.
- [46] Miskolczi N, Bartha L, Deák G. Thermal degradation of polyethylene and polystyrene from the packaging industry over different catalysts into fuel-like feed stocks. *Polymer Degradation and Stability*. 2006;91:517-26.
- [47] Aboulkas A, El harfi K, El Bouadili A. Thermal degradation behaviors of polyethylene and polypropylene. Part I: Pyrolysis kinetics and mechanisms. *Energy Conversion and Management*. 2010;51:1363-9.
- [48] Elordi G, Lopez G, Aguado R, Olazar M, Bilbao J. Catalytic Pyrolysis of High Density Polyethylene on a HZSM-5 Zeolite Catalyst in a Conical Spouted Bed Reactor. *International Journal of Chemical Reactor Engineering*. 2007;5:1-9.
- [49] Nishino J, Itoh M, Fujiyoshi H, Uemichi Y. Catalytic degradation of plastic waste into petrochemicals using Ga-ZSM-5. *Fuel*. 2008;87:3681-6.
- [50] Sarker M, Rashid MM. Production of Valuable Hydrocarbons by Catalytic Degradation of a Mixture of Polyvinyl Chloride and Polystyrene Waste. *International Journal of Engineering and Technology Research*. 2013;1:17-26.
- [51] Rashid MM, Sarker M. Liquid Fuels and Chemicals from Several Plastic Wastes and Motor Vehicle Tire Mixture by Catalytic Cracking. *American Journal of Environment, Energy and Power Research*. 2013;1:108-16.
- [52] Sarker M, Rashid MM. Hydrocarbon Compounds Fuel Recover from LDPE/HDPE/PP/PS Waste Plastics Mixture Using Zinc Oxide Catalyst. *International Journal of Sustainable Energy and Environment*. 2013;1:14-24.
- [53] Vasile C, Pakdel H, Mihai B, Onu P, Darie H, Ciocâlțeu S. Thermal and catalytic decomposition of mixed plastics. *Journal of Analytical and Applied Pyrolysis*. 2001;57:287-303.
- [54] Lee KH. Composition of aromatic products in the catalytic degradation of the mixture of waste polystyrene and high-density polyethylene using spent FCC catalyst. *Polymer Degradation and Stability*. 2008;93:1284-9.
- [55] Gobin K, Manos G. Thermogravimetric study of polymer catalytic degradation over microporous materials. *Polymer Degradation and Stability*. 2004;86:225-31.
- [56] Stelmachowski M. Thermal conversion of waste polyolefins to the mixture of hydrocarbons in the reactor with molten metal bed. *Energy Conversion and Management*. 2010;51:2016-24.
- [57] Sivakumar P, Anbarasu K. Catalytic Pyrolysis of Dairy Industrial Waste LDPE Film into Fuel. *International Journal of Chemistry Research*. 2012;3:52-5.



6th BSME International Conference on Thermal Engineering (ICTE 2014)

Scoping e-portfolios to engineering and ICT education

Firoz Alam, Harun Chowdhury*, Alex Kootsookos and Roger Hadgraft

School of Aerospace, Mechanical and Manufacturing Engineering, RMIT University, Melbourne, 3083, Australia

Abstract

E-portfolios are progressively becoming a key means for students to integrate their learning across the entire length of their program. However, the application of e-portfolios in engineering and ICT programs has been generally isolated to a few courses in each program, if at all. This paper summarises the use of e-portfolios to document student learning. Other aspects of the paper include the need for connections to curriculum mapping tools, e-portfolio software platforms, integration of outcomes through the curriculum, professional placements in industry, final year projects, etc.

© 2015 The Authors. Published by Elsevier Ltd.

Peer-review under responsibility of organizing committee of the 6th BSME International Conference on Thermal Engineering (ICTE 2014).

Keywords: e-portfolio; standards; accreditation; program learning outcomes; competencies.

1. Introduction

The delivery of higher education has been facing enormous changes and challenges over the last two decades with the progressive introduction of various educational technologies and tools that have affected all aspects of traditional teaching and learning [1, 2]. In this changing environment, engaging students is a difficult task faced by all academics [3-5]. Student engagement can be defined as a “student’s willingness, need, desire and compulsion to participate in, and be successful in, the learning process” [6, 7]. Electronic Portfolio or e-Portfolios may be used as a vehicle for addressing many problems including current assessment practices [8]. The use of e-Portfolio can enhance assessment and feedback and reflective learning especially where module-based exam assessments do not enable to provide feedback due to restricted access to exam scripts [6]. An e-Portfolio is defined as a portfolio of digital

* Corresponding author. Tel.: +61 3 99256103; fax: +61 3 99256108.

E-mail address: harun.chowdhury@rmit.edu.au

collection of individual and group demonstrations, resources, and accomplishments, team work, etc. via online or offline. An e-Portfolio contains 3 main sections: a) a storage area to store and / or archive evidence or artifacts, b) a reflection area which can be shared with others for public comments/ feedback, and c) a presentation or public area where one can present himself/herself to different people for different purposes. The electronic evidence may include stored text, files, images, audio/video clips, blog entries, twitter and social media texts, and various web links. The e-Portfolio is generally planned, developed and compiled by the owner. Usually there are 3 main categories of information broadly compiled in e-Portfolios: a) Personal Details - personal information, personal values and interests, personal activities – volunteer work, professional development, hobbies and interests, personal reflections, etc., b) Academic Records - education history, subject related matters such as assignment, projects, papers, etc., academic staff comments, peer comments, learning reflections, etc., and c) Career - goals and plans, work history, curriculum vitae/ resume, awards and certificates, reflective manager comments and/ or peer comments, etc. In higher education, students prepare the e-Portfolios and the academic staff member assesses it. E-Portfolio is a kind of actual evidence of learning process and learning achievement. E-Portfolio allows sharing the information with other making it a powerful tool in personal and professional development.

2. E-Portfolios in higher education

There are at least three types of e-Portfolios are widely used. They are: a) home-grown (institution specific), b) open source (institute and/ companies developed), and c) commercial. E-portfolios can also be sub-grouped based on their features and purposes such as a) developmental portfolios, b) assessment portfolios, and showcase portfolios as shown in Table 1.

Developmental Portfolio - it demonstrates the advancement and development of student's skills over a period of time. It is considered works-in-progress and includes both self-assessment and reflection/feedback elements. The main objective of this portfolio is to provide communication between students and academic staff.

Assessment Portfolio - it shows student's competence and skill for particular and specialised areas. This portfolio can be used for ongoing and/or end of subject/course and program assessment for assessing student performance. The primary aim of this type of portfolio is to examine student competency as outlined by the course/subject and program learning outcomes and standards.

Showcase Portfolio – it illustrates student's skills and work examples. Usually, the showcase portfolio is created at end of a course/subject and /or program to show the quality of student's work. This portfolio can be used by the student to his/her potential employers to gain employment at the end of a program.

Now a day, most e-Portfolios are hybrid types encompassing features of developmental, assessment and showcase portfolios.

Table 1. E-Portfolio types based on features and purposes (adapted from <http://scu.edu.au/teachinglearning/index.php/79>).

Types of e-Portfolios	Features	Purposes
Developmental (learning, reflection, formative, work in progress)	<ul style="list-style-type: none"> • Focus on the learning 'process' and work in progress • Features self-assessment, formative feedback and reflection 	<ul style="list-style-type: none"> • Formative feedback on learning • Develop communication and reflective skills
Showcase (professional, formal, presentation, career, employment)	<ul style="list-style-type: none"> • Focuses on the 'product' • Features exemplary work and skills • Illustrates and evidences experience /achievements 	<ul style="list-style-type: none"> • Demonstrate quality of work and achievements • Showcase skills to employers/clients
Assessment (summative formal assessment)	<ul style="list-style-type: none"> • Evidence of competency or accreditation standards 	<ul style="list-style-type: none"> • Evaluate competency and achievements against criteria or standards
Institutional (also called planning, continuous professional development, or academic e-Portfolios).	<ul style="list-style-type: none"> • Reflection on professional progress • Professional development planning • records achievements, plans and non-professional activities 	<ul style="list-style-type: none"> • Document ongoing professional learning

Some widely cited e-Portfolio platforms are: a) Desire2Learn, b) Digication, c) E-scape, d) Educa, e) Elgg, f) Equal Electronic Portfolio, g) Foliotek, h) LiveText, i) Mahara, j) MAPS, k) OpenSchool ePortfolio, l) Passport, m) Pathbrite, n) PebblePad, o) RCampus, p) Taskstream.

However, Mahara, PebblePad and Foliotek are widely used in higher education. In Australia, RMIT University, La Trobe University, Charles Sturt University, Flinders University, Murdoch University, University of Sydney, University of Tasmania, Bond University, James Cook University, Edith Cowan University, University of Western Sydney, and Victoria University are using PebblePad platform as e-Portfolio. In addition, Australian Library and Information Association, the Australian Physiotherapy Association, Technical and Further Education (TAFE) of South Australia, Ranges TEC, and Royal District Nursing Service of South Australia also use PebblePad e-Portfolio for their members [9]. In New Zealand, the Wellington Institute of Technology and Osteopathic Council of New Zealand are the user of PebblePad e-Portfolio platform.

The utilisation of e-portfolios by students in their learning offers numerous benefits. E-Portfolios enable students to explore and take decision on their learning and prepare themselves for the future. The e-Portfolio assists in developing ongoing, evidence-based learning and performance assessment throughout a course/subject and/or a program. Some important advantages that an e-Portfolio can offer are:

- Space for feedback that can be used for performance improvement and saved for future use;
- Initiative to be self-directed and responsible for student's own learning and assessment;
- Opportunity to make connections between tacit knowledge and constructed knowledge;
- track students' accomplishments and feedback over a sustained period, through on going assessment;
- Digital literacy skills development;
- Communication skills specially for international students;

An e-Portfolio should have four important features: a) flexible structure, b) opportunities for self-reflection, c) support for career development, and d) reflection and feedback on learning

3. E-Portfolios at RMIT University

RMIT is currently using PebblePad as an e-Portfolio tool. PebblePad is a web-based e-Portfolio system which allows students to store, package and present their learning, goals and achievements for different purposes (assessment, personal, career development, etc.). Various features and tools in PebblePad platform are illustrated in Figure 1.

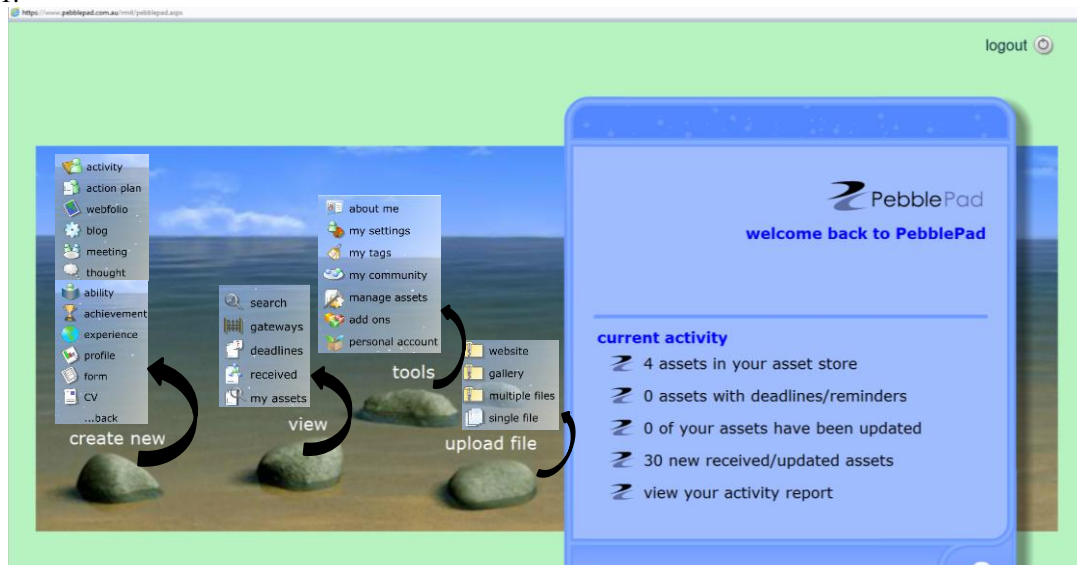


Fig. 1. PebblePad input features.

PebblePad provides a Personal Learning Space. It is a web based program that offers a number of different tools to plan work, organise evidence of learning and record and reflect on learning. PebblePad has two main sections: a) Pebble+ and b) ATLAS as shown in Figure 2. Pebble+ area is a private area where one can create and store assets and learning contents whereas ATLAS area is for assessment space where one can submit selected assets for assessment, grading and feedback. PebblePad space is password protected, all the work students undertake are their own and confidential. When students are ready to publish an asset they can send it to a workspace that allows their lecturer(s) or peers to view and comment on their work.

Students from different programs and schools across RMIT University can use PebblePad as e-Portfolio tool. All students in the School of Aerospace, Mechanical and Manufacturing Engineering of RMIT University have access to a PebblePad account whilst they are enrolled in their final year research project course at the University. PebblePad has many uses but at RMIT University its primary purpose is to collect and create evidence of students learning in the form of journals, blogs, web-folios, photos, documents, media files, industry work experience report, minutes of weekly meeting between final year project supervisor(s) and students, and links to external web sites from Pebble+. Students can then use the different types of evidence to creatively build assets in Pebble+ and submit these as assessment tasks to ATLAS as per the instruction of the lecturer and/or course guides as shown in Figure 2. These students' assets can be shared with prospective employers and other external parties.

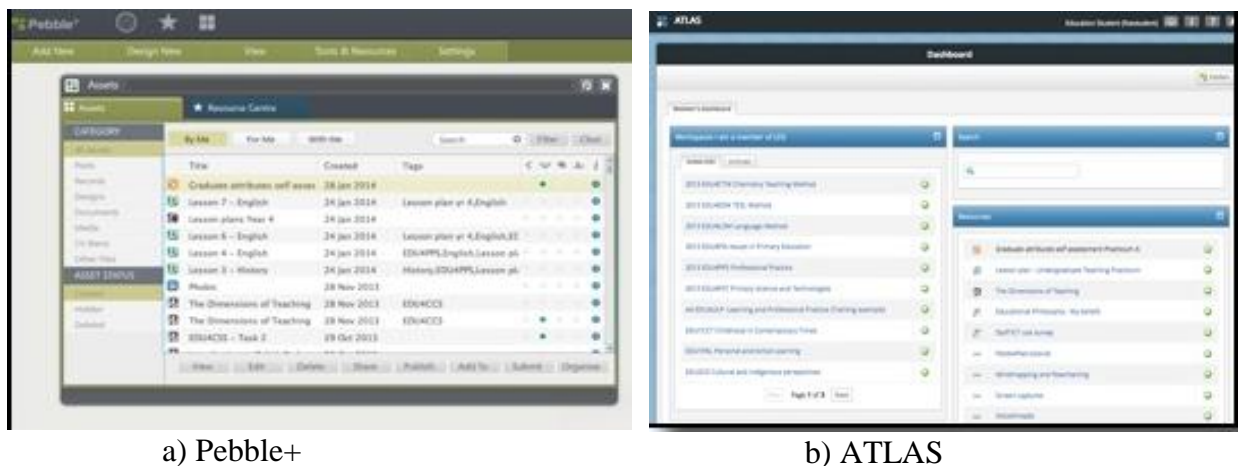


Fig. 2. Work areas in PebblePad (adapted from [10]).

E-Portfolios are excellent tools for showing the development of students' skills and abilities in both formal and informal contexts. The evidence of these skills (course or subject matter skills, communication skills, team work skills, professional practice skills, etc.) can be used for the career development and employment. To enhance employability of graduates, RMIT University has developed a Career Track for students to incorporate their CVs and individual career planning in e-Portfolio that can be linked to PebblePad and similar platforms. Fig. 3 shows an e-portfolio platform that can be used for individual student's career development profile at RMIT University.



Fig. 3. Career development using e-portfolio (www.rmit.edu.au).

4. Challenges in e-Portfolio utilisation

In order to utilise the full potential of e-Portfolios in higher education especially in engineering and ICT, both students and academic staff members need to overcome many challenges including: i) investment of time by both students and academic staff, ii) technical proficiency of students and academic staff, and iii) development of students ability for critical reflection and selection of work for assessment. In e-Portfolios, both students and academic staff are required to engage in individual and collaborative activities and cultivate interactive culture.

4.1. Challenges for students

The challenges for students in utilisation of e-Portfolios in their learning are mainly the anticipated additional time and workload. Students need additional assistance to develop e-Portfolio platform/software user skills, technical (subject matter) skills, and skills of selection, collection, and reflecting on learning materials. Students may also need advice on appropriate use of a typical e-Portfolio environment and space. They also need to have access to internet during their study time so that they can login into the e-Portfolio platform uninterrupted which is considered to be a challenge due to occasional system outages and site maintenance.

4.2. Challenges for academic staff

The challenge for academic staff in e-Portfolio uses is mainly the modification time and effort required to the traditional assessment practices for an individual course or subject. These modifications of assessment practice for e-Portfolios are time consuming and required additional skills including computer skills for variable class size (large class and small). The assessments are subjective and the modification may compromise assessment reliability due to use of incorrect assessment rubrics and marking schemes. Academic staff needs careful consideration in assessing e-Portfolio as it takes time for students to become familiar with the e-Portfolio idea. The process of collecting, selecting and reflecting on learning materials possesses a great challenge too. Another challenge for academic staff is to provide feedback to students on time as the late assessment of student's e-Portfolios in the course/subject can jeopardise students learning outcomes.

5. Discussion and future strategy

In order to achieve a sustained impact, e-Portfolios should be used by higher education institutions especially engineering and technology focussed institutions, academic staff, students, professional accreditation bodies so that students can effectively use throughout their programs (study) and for job applications and leading into e-chartered, review of e-portfolio extracts by accreditation panels and use of e-portfolio extracts by employers. Therefore future strategy should be on e-Portfolios that incorporate ‘assessment equivalence of qualifications and learning outcomes’, ‘assessment and promotion of learning’ and ‘employability skills’. The following features of a typical e-Portfolio should be included for the wider use:

- Flexibility so that professional competencies and skills requirements can be added for the information age with convenient many-to-many tagging
- User capability by students throughout their programmes and afterwards
- Inter-operability of e-portfolios i.e. facility to carry the e-portfolio after graduation and throughout a career
- Easy connection to professional organisations especially engineering accreditation bodies
- Support system for reflective practice
- Facility to link to assessment
- Modelled use and demonstrated value by academics
- Capability for peer mentor development
- Ability for industry-based mentor development
- Capacity for extracting a standardised portfolio for employment opportunity

By integrating all above mentioned dot point features, an e-Portfolio across a program can be a means to support widening participation of traditional and non-traditional students/learners of all teaching modes (face to face, distance and hybrid), international students, distance learners, and learners who are work-based or engaged in continuous professional development. As the number of student mix (local and international) in higher education especially in engineering is constantly increasing, managing diverse cohorts and teaching large groups have become a challenge for academic staff member. The utilisation of e-Portfolios can overcome this challenge. In order to enhance employability skills as well as professional accreditation of an academic program, e-Portfolios can be used to map competencies across the curriculum and students’ attainment against these competencies. E-portfolios can also be used to keep transparent records for learning pathways, credit transfers, and multiple modes of participation and assessment. In the long run, the use of e-Portfolios can mitigate current challenges in higher education especially in engineering if a common e-portfolio platform can be used by universities, accreditation bodies, and work placements (industry employers).

References

- [1] Alam, F., Hadgraft, R. and Alam, Q. (2014), eLearning – Challenges and Opportunities, in: *Using Technology Tools to Innovate Assessment, Reporting, and Teaching Practices in Engineering Education*, (ed. Alam F), IGI Global, New York.
- [2] Alam, F., Alam, Q., Chowdhury, H. and Steiner, T. (2013), *Transnational Education: Benefits, Threats and Challenges*, *Procedia Engineering*, Vol. 56: 870-874.
- [3] Harper, S. R., and Quaye, S. J. (2009). *Student engagement in higher education: Theoretical perspectives and practical approaches for diverse populations*. London, UK: Routledge.
- [4] Heafner, T. (2004), Using technology to motivate students to learn social studies. *Contemporary Issues in Technology and Teacher Education*, 4(1). Retrieved from <http://www.citejournal.org/vol4/iss1/socialstudies/article1.cfm> on 27 October 2014.
- [5] Trowler, V. (2010), *Student engagement literature review*. York, UK: Higher Education Academy.
- [6] O’Keeffe, M. and Donnelly, R. (2013), Exploration of ePortfolios for Adding Value and Deepening Student Learning in Contemporary Higher Education, *International Journal of ePortfolio*, Vol. 3 (1): 1-11
- [7] Bomia, L., Beluzo, L., Demeester, D., Elander, K., Johnson, M., and Sheldon, B. (1997), *The impact of teaching strategies on intrinsic motivation*. Champaign, IL: ERIC Clearinghouse on Elementary and Early Childhood Education.
- [8] Chatham-Carpenter, A., Seawel, L., and Raschig, J. (2010), Avoiding the pitfalls: Current practices and recommendations for ePortfolios in higher education, *Journal of Educational Technology Systems*, Vol. 38(4): 437-456.
- [9] Australasian PebblePad User Group: <https://www.pebblepad.com.au/australia/viewasset.aspx?oid=16412&type=webfolio>, accessed on 27 October 2014.
- [10] La Trobe University, e-portfolio: http://tlweb.latrobe.edu.au/education/ICTtools/pebblepad/PebblePad_010.html.



6th BSME International Conference on Thermal Engineering (ICTE 2014)

Characterization of Carbon Fiber Reinforced Epoxy Composites Modified with Nanoclay and Carbon Nanotubes

Md Ekramul Islam, Tanjheel H. Mahdi, Mahesh V. Hosur^{*}, Shaik Jeelani

Department of Materials Science and Technology, Tuskegee University, Tuskegee, Alabama-36088, USA

Abstract

Fiber reinforced polymer composites show significantly superior performance over many traditional metallic materials because of their superior strength to weight ratio and higher stiffness. Enhancement of properties of FRP composites can be possible by the modification of matrix properties. Significant development in the use of nanoparticles for modification of epoxy matrix has led to improved mechanical properties of the FRP composites. In this study, carbon fiber reinforced epoxy composites were modified with 2 wt.% Montmorillonite nanoclay and 0.3 wt.% multi-walled carbon nanotubes (MWCNTs). 3 point bending test, Dynamic Mechanical Analysis (DMA) and low velocity impact test (LVI) were conducted for characterizing modified samples. Results obtained from these experiments were compared with unmodified carbon/epoxy composites. Reinforcement with nanoparticles was found to significantly improve the mechanical and thermo-mechanical properties of carbon fiber reinforced polymer (CFRP) composites.

© 2015 The Authors. Published by Elsevier Ltd.

Peer-review under responsibility of organizing committee of the 6th BSME International Conference on Thermal Engineering (ICTE 2014).

Keywords: Polymer composites; nanoparticles; MWCNTs, Nanoclay; Mechanical characterization

1. Introduction

For the past several years, fiber reinforced polymer (FRP) composite materials are being considered for replacing the metallic components in aviation, naval and automotive industries. Compared to metal, FRP composites have low

□ Corresponding Author, Tel. +1-334-724-4220, Fax:+1-334-724-4224
E-mail address: hosur@mytu.tuskegee.edu

density, higher specific strength and stiffness, higher corrosion resistance and improved fatigue performance. Performance of these FRPs under various loading condition; such as axial, torsional and impact loading is very crucial for the design of structural components. Mechanical properties of fiber reinforced polymer composites depend on the fiber, matrix and the interface between them. Researchers have been investigating various organic and inorganic nanoparticles as reinforcement of composites to enhance the mechanical properties and thermal stability. Significant development in the use of nanoparticles for modification of epoxy matrix has led to improved mechanical properties of the FRP composites. The advantages of nanoparticles are their high specific strength and modulus along with low density. As a result, very low percentage of nanoparticles addition can enhance the properties of composites significantly.

Nomenclature

A	FRPC- Fiber Reinforced Polymer Composites
B	CFRP- Carbon Fiber Reinforced Polymer
C	CNTs- Carbon Nanotubes
D	MWCNTs- Multi-Walled Carbon Nanotubes
E	MMT- Montmorillonite Nanoclay

Among the nanoparticles, carbon nanotubes (CNTs) are the strongest materials known to man and are most widely used because of their strong interfacial interactions and excellent stress transfer properties. In their study Cooper et al. [1] demonstrated that the effective modulus of MWCNTs dispersed in a composite could be about 1 TPa and that of the SWCNTs more than 1 TPa. Schadler et al. [2] tested multiwalled nanotube/epoxy composites under tensile and compressive loading and found the compressive modulus of the composites to be higher in MWCNT modified composites compared to the neat composites. To employ CNT as effective reinforcements in polymer composites, uniform dispersion and proper interfacial adhesion between polymer and CNTs is most important issue. Researchers also found that the chemical functionalization of MWCNT surfaces increases the compatibility between epoxy matrix and CNT due to the formation of an interface with stronger interconnections [3]–[5]. Functionalization of MWCNTs with COOH- group lead to better performance at higher loading rates (5 wt. %) compared amino groups (NH₂) [6]. COOH-MWCNT nanocomposites resulted in 50% improvement in the tensile strength and 35% improvement in the Young's Modulus over the neat polymeric composites. COOH functionalization helps to achieve better interfacial reaction between MWCNTs and the epoxy matrix resulting in better dispersion [7]. This better dispersion of MWCNTs effects the improvement of mechanical properties of polymeric composites. COOH in MWCNTs creates interconnection with polymer matrix and therefore make the nanocomposites more resistant to chemical attack [3]. Kostopoulos et al. [8] and Solaiman et al. [9] showed that addition of MWCNTs in CFRP composites increased the impact damage resistance.

However, CNTs are expensive and can be hazardous to health [10]. Less expensive organic materials like nanoclays are also popular for composite reinforcement. Nanoclays are layered structures capable of reinforcing the matrix to enhance mechanical properties. They act as thermal and moisture barrier to provide thermal stability and environmental degradation resistance as well. Thermal and mechanical behavior of clay-epoxy composites are investigated by numerous researchers and they obtained best mechanical properties for 2 wt. % of nano-clay reinforcement [11], [12]. Nanoclay creates a labyrinth or tortuous path for moisture absorption which effectively enhances the barrier property of polymer nanocomposites [13]. The large aspect ratio of nano-fillers increases the effective penetration path and reduces permeability. Bagherzadeh et al. [14] found increasing barrier and anti-corrosive properties with increasing clay content with about 70% reduction in water uptake at 1 wt.% clay loading. Among the clay minerals of the smectite group, montmorillonite nanoclay has been most widely used for the preparation of polymer clay nanocomposites [15]. However, the surface of the nanoclay needs to be modified with organophilic materials in order to make compatible with organic polymers and increase moisture barrier properties.

In this study, 0.3 wt.% COOH-MWCNTs and 2 wt.% I30E (Octadecylamine surface modified) Montmorillonite Nanoclay have been added to carbon fiber reinforced epoxy composites. 3 point bending (flexure) test, Dynamic Mechanical Analysis (DMA), and Low Velocity Impact (LVI) test have been conducted to characterize the modified composites and then compared with unmodified carbon/epoxy composites.

2. Materials and methods

2.1. Materials

In this study, carbon fiber reinforced epoxy composites serves as control samples. The carbon fiber used as reinforcement was 8 hrs satin weave (8" HS) with tow size 3k and thickness of 0.4572mm, supplied by US composites. The resin used was SC-15 epoxy resin which consists of two parts; part A: diglycidyl ether of bisphenol A, and part B: cyclo aliphatic amine hardener with a stoichiometric ratio of A:B=10:3. The COOH functionalized multi-walled carbon nanotubes had a diameter of 10-20nm and length of 10-30 micrometer. Montmorillonite nanoclay was surface modified and contains 25-30 wt. % octadecylamine.

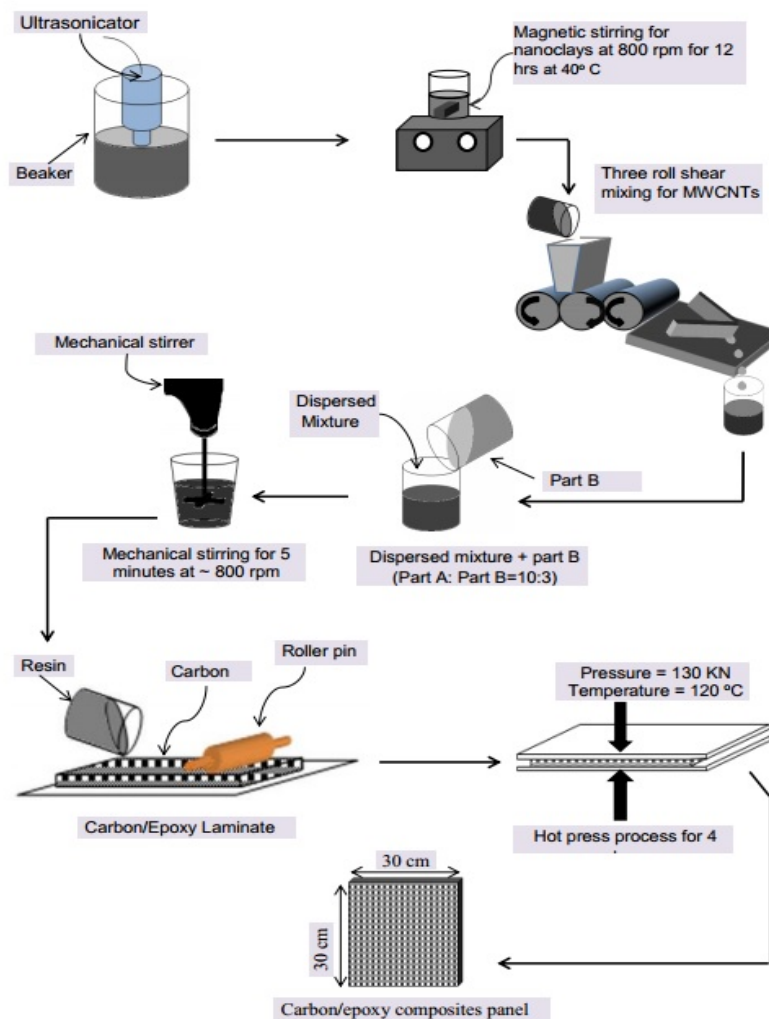


Fig. 1. Dispersion of nanoparticles and fabrication of laminates

2.2. Dispersion of nanoparticles

Different techniques were used for proper dispersion of these nanoparticles in epoxy matrix. Figure 1 shows the dispersion techniques and composite fabrication procedure. 0.3 wt% of MWCNTs were measured and mixed with part A of SC-15 resin by mechanical mixture. The mixture was subsequently ultra-sonicated for 30 minutes at 40° C. To facilitate the dispersion and minimize the agglomeration, three roll shear mixture was then used. The maximum speed of the roller was maintained at 150 rpm and three passes through the rollers were conducted with roller gap of 20µm (first pass), 10µm (second pass) and 5µm (final pass). For achieving a uniform dispersion and completely exfoliated nanoclay in epoxy resin, sonication and magnetic stirring were preferred over other methods. 2 wt.% I30E nanoclay was weighed and mixed with the resin using mechanical mixture. Ultra-sonication was then conducted for 30 minutes at 40° C. After that the mixture was magnetically stirred at about 800 rpm for 12 hours.

2.3. Laminate fabrication

After dispersion, nanoparticle incorporated epoxy SC-15 part A was mixed with part B at a ratio 10:3. Carbon fiber-epoxy composites were fabricated by a combination of hand lay-up process and compression molding technique. Eight layers of carbon fiber sheets were stacked one after another with resin layers between them. The hand laid-up system was then placed inside the compression mold, for 4 hours. During the compression molding process, a pressure of 130 KN was applied and the temperature was maintained at 120° C to obtain completely cured carbon-epoxy composites. The thickness of the laminates obtained was about 2.42mm.

2.4. Characterization techniques

Fiber reinforced composites were subjected to various tests to obtain the mechanical, thermal and viscoelastic properties. Properties obtained from nanoparticles modified composites were compared with those of control samples.

Flexure test was conducted according to ASTM D790-02. The test was conducted in three-point bending configuration using a Zwick-Roell machine. The test was performed at a rate 1.2 mm/minute under displacement control mode. The sample size was maintained according to the ASTM, where span length to thickness ratio is 16:1. The sample size was 60 mm × 12.5 mm × 2.5 mm.

Viscoelastic properties of fiber reinforced composites are obtained from dynamic mechanical analysis. DMA tests were conducted according to ASTM D4065-12 using TA instrument DMA Q 800. The tests were performed in three point bending mode at a frequency 1 Hz and amplitude 15 µm. The temperature ramp was 10° C/minute within the range 30° C and 180° C. The sample size was 60 mm × 13 mm × 3 mm for the test.

Low velocity impact tests were conducted by a DYNATUP 8210 drop weight impact testing machine. The energy and velocity was varied by changing the weight and height of the dropping weight of the impactor. The height and weight of impactor was changed to strike the samples with 30J, 40J and 50J energy. The machine also records velocity, deflection energy and load as functions of time. Peak load, time to attain the peak load and deflection of samples at peak load were observed from the data acquired and compared for different samples. Other related parameters like absorbed energy were calculated from area under the load versus deflection curve.

A cutting edge thermal imaging instrument was used to qualify and quantify the damages on the samples. A bright flash goes on for a split second and an infrared camera captures the heat signature as the surface cools down. Detection of anomalous cooling due to extremely large or shallow features may be performed by viewing the raw image data from the infrared camera [16]. The first and second logarithmic derivative data is used for reducing noise in raw image signal. The obtained colored images were then converted to a black and white image which clearly differentiates the damaged and undamaged portions. Finally, damage area was calculated using MATLAB coding from this image by taking percentage of black portion of the image as function of the total area.

3. Results and Discussion

3.1. Flexural properties

Carbon fiber reinforced composites modified with nanoparticles are subjected under three point bending load to compare the flexural properties of nanoparticles modified ones to control one. Flexural stress versus strain plots are depicted in figure 2 which shows the influence of nanoparticles on the flexural properties of composites. Related data accumulated is tabulated in table 1. Flexural strength and modulus of all the samples increased with addition of nanoparticles and the improvement were almost similar.

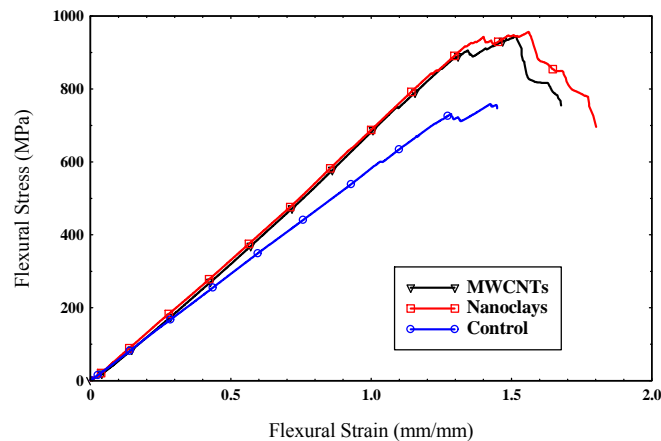


Fig. 2. Flexural Stress versus strain response of control and nanoparticles reinforced carbon fiber/epoxy composite samples

Table 1. Flexure test results of control and nanoparticles reinforced carbon fiber/epoxy composites

Sample type	Flexural Strength, MPa	% Change	Flexural Modulus, GPa	% Change	Strain at maximum stress	% Change
Control	799.63±51.83	-	56.58±2.62	-	1.53 ± 0.15	-
Nanoclay Reinforced	961.54±18.93	20	68.61±1.07	21	1.54 ± 0.05	1
MWCNT reinforced	953.71±12.32	19	64.85±2.56	15	1.54 ± 0.19	1

3.2. Dynamic mechanical analysis(DMA)

Nanophased and control carbon fiber/epoxy composites were subjected under dynamic mechanical analysis to obtain viscoelastic properties. Storage modulus and loss modulus as a function of temperature are plotted in figure 3. Peak storage modulus, loss modulus and tan-delta values as well as glass transition temperature are displayed in table 2. The standard deviation of all peak value was trivial. From the figure and table it is evident that nanoparticles reinforced carbon fiber/epoxy composites possess higher storage modulus and glass transition temperature than control composites. Moreover, nanoclays reinforced composites had higher storage modulus, yet lower glass transition temperature. On the contrary, MWCNTs reinforced composites exhibited lower storage modulus, yet high glass transition temperature. Loss modulus and damping properties of nanophased composites are also much higher than control composites. When the load is applied, the nanoparticles try to hold the laminae in place, so more amount of energy is required to deform the samples.

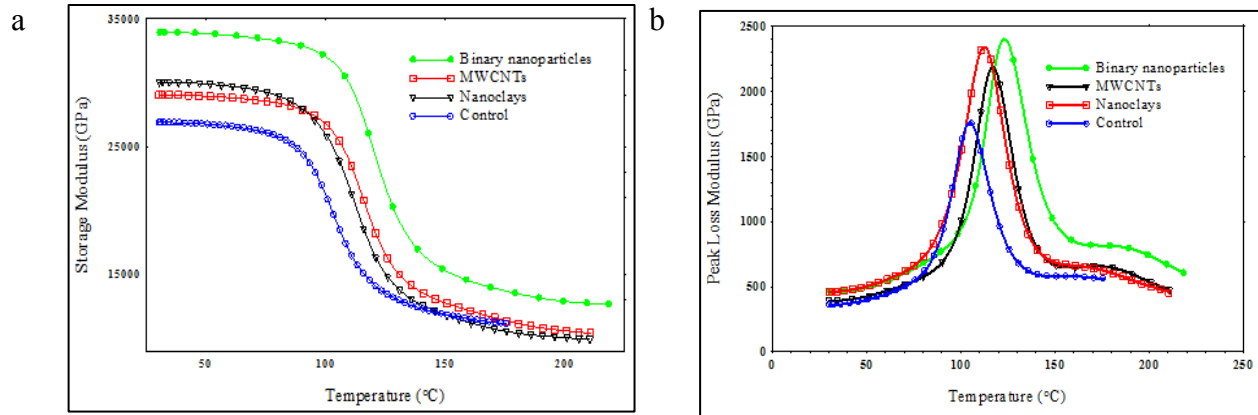


Fig. 3. (a) Storage modulus; (b) Loss modulus of modified and control carbon/epoxy composites.

Table 2. DMA results of control and nanoparticles reinforced carbon fiber/epoxy composites

Sample Type	Storage modulus, MPa	% Change	Peak loss modulus, MPa	% Change	Glass Transition Temperature, °C	% Change
Control epoxy resin	25460.25 ± 1302.86	-	1725.95 ± 60.59	-	107.67 ± 1.55	-
Nanoclays reinforced	30105.3 ± 78.63	18	2374.74 ± 25.13	38	120.36 ± 0.76	12
MWCNTs reinforced	29020.5 ± 757.51	14	2215.32 ± 116.77	30	116.31 ± 2.36	8

3.3. Low velocity impact (LVI)

Low velocity impact tests were conducted for control and all kinds of nanoparticles modified samples at 30J and 40J energy levels and Load vs displacement curves were plotted (figure 4). It was found that before conditioning, all kinds of modification showed better performance than control samples. At 30J energy level the load-displacement profile was very smooth for all samples indicating no sudden lamina failure. On the contrary, tests conducted at 40J energy levels shows sudden drop of the profile for all samples.

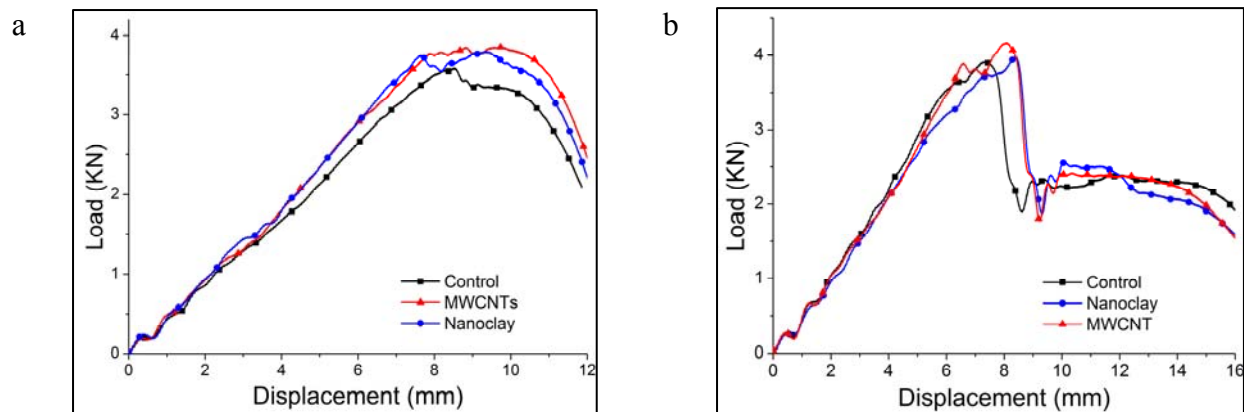


Fig. 4. (a) Load vs Displacement plot for control and modified carbon/epoxy composites impacted at (a) 30J; (b) 40J energy levels.

Absorbed energy is a significant parameter, which can be calculated from the area under the load vs. deflection curve. When the sample reaches to its maximum elastic limit, it absorbs the excess energy in the form of plastic

deformation and damaging mechanism. Since the nano-composites are brittle in nature, no plastic deformation takes place; the excess energy is utilized to damage the composites. Table 3 shows the absorbed energy of the samples and the nanoparticles modified samples showed improvement over the control samples. The damage area of the impacted samples were calculated from thermoscopy images (figure 5) and presented in table 4. The damage area was reduced by modification of epoxy matrix with nanoparticles.

Samples	30J	40J
Control	26.03 ±0.34	38.10 ±0.37
Nanoclay modified	29.11 ±1.34	41.05 ±0.23
MWCNTs modified	31.15 ±1.36	41.87 ±0.06

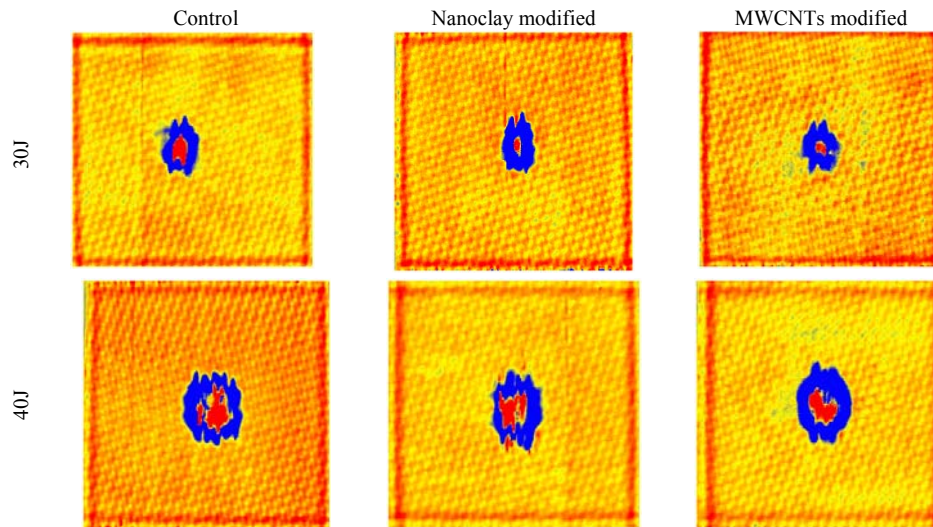


Fig. 5. Thermoscopic images of control and modified carbon/epoxy composites.

Impact Energy	Damage	Control	Nanoclay modified	MWCNTs modified
30 J	Area	38.47	25.39	21.97
	% reduction	-	34.01	42.88
40J	Area	117.33	82.63	78.65
	% reduction	-	29.58	32.97

4. Conclusions

Modification of epoxy matrix with COOH-MWCNTs and montmorillonite Nanoclay was found to improve the mechanical and thermo-mechanical properties of carbon fiber reinforced epoxy composites.

- Improvement of flexure strength, modulus and strain at failure was almost similar for both kinds of nanoparticles.
- Composites reinforced with nanoclay had higher storage modulus, while MWCNTs reinforced composites exhibited higher glass transition temperature. Loss modulus and damping properties of nanophased composites are also much higher than control composites.

- In case of low velocity impact test, the nanoparticles modified samples were able to absorb higher amount of energy. Also the damage area was reduced while compared to control samples. MWCNTs modified samples showed better impact resistance.

Acknowledgements

This material is based upon work supported by, or in part by, the U. S. Army Research Laboratory and the U. S. Army Research Office under contract/grant number (W911NF-12-1-0053), NSF-EPSCoR (EPS 1158862) and NASA-EPSCoR (NNX10AN26A).

References

- [1]. C. A. Cooper, R. J. Young, M. Halsall, Investigation into the deformation of carbon nanotubes and their composites through the use of Raman spectroscopy, *Compos. Part A Appl. Sci. Manuf.* 32 (Mar. 2001) 401–411.
- [2]. L. Schadler, S. Giannaris, P. Ajayan, Load transfer in carbon nanotube epoxy composites, *Appl. Phys. Lett.* 73 (1998) 3842–4.
- [3]. L. Guadagno, B. De Vivo, a. Di Bartolomeo, P. Lamberti, a. Sorrentino, V. Tucci, L. Vertuccio, V. Vittoria, Effect of functionalization on the thermo-mechanical and electrical behavior of multi-wall carbon nanotube/epoxy composites, *Carbon N. Y.* 49 (May 2011) 1919–1930.
- [4]. Z. Yaping, Z. Aibo, C. Quinghua, Z. Jiaoxia, N. Rongchang, Functionalized effect on carbon nanotube/epoxy nano-composites, *Mater. Sci. Eng. A* 435–436 (2006) 145–149.
- [5]. N. Sahoo, S. Rana, J. Cho, L. Li, S. Chan, Polymer nanocomposites based on functionalized carbon nanotubes, *Prog. Polym. Sci.* 35 (2010) 837–867.
- [6]. B. Singh, D. Singh, R. Mathur, T. Dhama, Influence of surface modified MWCNTs on the mechanical, electrical and thermal properties of polyimide nanocomposites, *Nanoscale Res. Lett.* (2008).
- [7]. N. Jahan, A. Narteh, M. Hosur, Effect of Carboxyl Functionalized MWCNTs on the Cure Behavior of Epoxy Resin, *Open J. Compos. Mater.* 2013 (2013) 40–47.
- [8]. V. Kostopoulos, A. Baltopoulos, P. Karapappas, A. Vavouliotis, A. Paipetis, Impact and after-impact properties of carbon fibre reinforced composites enhanced with multi-wall carbon nanotubes, *Compos. Sci. Technol.* 70 (Apr. 2010) 553–563.
- [9]. E. M. Soliman, M. P. Sheyka, M. R. Taha, Low-velocity impact of thin woven carbon fabric composites incorporating multi-walled carbon nanotubes, *Int. J. Impact Eng.* 47 (Sep. 2012) 39–47.
- [10]. Jia Du, S. Wang, H. You, X. Zhao, Understanding the toxicity of carbon nanotubes in the environment is crucial to the control of nanomaterials in producing and processing and the assessment of health risk for human: A review, *Environ. Toxicol. Pharmacol.* 36 (2013) 451–462.
- [11]. R. Hegde, Structure and properties of nanoclay reinforced polymer films, fibers and nonwovens, *Dr. Diss.* (2009).
- [12]. F. H. Chowdhury, M. V. Hosur, S. Jeelani, Studies on the flexural and thermomechanical properties of woven carbon/nanoclay-epoxy laminates, *Mater. Sci. Eng. A* 421 (Apr. 2006) 298–306.
- [13]. A. A. Azeez, K. Y. Rhee, S. J. Park, D. Hui, Epoxy clay nanocomposites – processing, properties and applications: A review, *Compos. Part B Eng.* 45 (Feb. 2013) 308–320.
- [14]. M. R. Bagherzadeh, F. Mahdavi, Preparation of epoxy–clay nanocomposite and investigation on its anti-corrosive behavior in epoxy coating, *Prog. Org. Coatings* 60 (Sep. 2007) 117–120.
- [15]. S.-I. Hong, H.-H. Lee, J.-W. Rhim, Effects of clay type and content on mechanical, water barrier and antimicrobial properties of agar-based nanocomposite films, in *The 11th International Congress on Engineering and Food (ICEF)*, (2011).
- [16]. S. M. Shepard, J. R. Lhota, T. Ahmed, Flash thermography contrast model based on IR camera noise characteristics, *Nondestruct. Test. Eval.* 22 (Jun. 2007) 113–126.

6th BSME International Conference on Thermal Engineering (ICTE 2014)

Strain energy release rate and mode-I delamination growth in carbon-graphene/epoxy hybrid nanocomposites

David A. Hawkins Jr.^a and Anwarul Haque^{a*}

^a*The University of Alabama, 245 7th Avenue, Tuscaloosa, AL 35401, USA*

Abstract

The influence of graphene reinforcement in strain energy release rate (G_{IC}) and Mode-I delamination growth in carbon-graphene/epoxy (CG-Ep) hybrid nanocomposites have been studied using the double cantilever beam (DCB) test. The specimens of carbon/epoxy (C-Ep) and CG-Ep nanocomposites were manufactured using vacuum assisted manual lay-up method. DCB tests were conducted in a displacement controlled mode to achieve stable delamination growth under static loading. At the onset of delamination growth, the load (P_{cr}) and the total opening displacement (δ_{cr}) were recorded. The total compliance of the DCB specimen was obtained using, $C = \delta/P$. P_{cr} and δ_{cr} are recorded as a function of the delamination length (a). Plots of critical loads and compliances as a function of the delamination size were used in computing G_{IC} , the Mode-I critical strain energy release rate. The delaminated zone was studied through fractographic examinations and surface roughness measurement. The results show improved G_{IC} of CG-Ep nanocomposites in comparison to traditional C-Ep composites. The fractured surface of CG-Ep shows undulated surface with increased roughness which possibly contributed in crack deflection mechanisms.

© 2015 The Authors. Published by Elsevier Ltd.

Peer-review under responsibility of organizing committee of the 6th BSME International Conference on Thermal Engineering (ICTE 2014).

Keywords: Strain energy release rate; delamination growth; nanocomposites; graphene nanoparticles; double cantilever beam;

* Corresponding author. Tel.: 1-205-348-2694;
E-mail address: ahaque@eng.ua.edu

1. Introduction

Composite materials have gained significant importance in many engineering structures and industry applications over the last few years. Specifically, the aerospace, automotive, and maritime industries continue to utilize a wide variety of composite materials in a number of industrial and commercial applications. The exceptional strength to weight ratios presented by many advanced composite materials are desirable for industries that constantly fight to improve efficiency. Most prominent among these materials is carbon fiber. Carbon fiber composites have become important lightweight structural materials in many engineering applications. While carbon fiber presents many outstanding physical characteristics, there always remains the possibility of improving existing material systems. To enhance the properties of existing composites, nanoparticles can be integrated into composite specimens.

Recently, graphene has become a promising nanofiller material for a variety of composite applications [1-2]. Graphene presents amazing physical characteristics and has been shown to be effective at improving mechanical, electrical and thermal properties of a number of composite materials. The performance of laminated composites is also significantly depends on the interlaminar fracture energy which eventually controls the delamination crack growth in fiber reinforced composite. Many studies have been done to analyze the performance of composites in this aspect [2-8]. The critical strain energy release rate (G_{IC}) is an important material property which controls the crack propagation in composite structures. It has been reported that G_{IC} of baseline epoxy is significantly enhanced by adding very little quantity of graphene (0.1% by weight) filler materials. Such enhancement in fracture energy in graphene/epoxy(G-Ep) nanocomposites shows potential to reduce delamination crack growth in traditional C/Ep composites provided G-Ep is used as resin materials. In fact, a three-phase composite such as CG-Ep is more applicable in structural load bearing components than a two phase G-Ep system.

The goal of this study is to examine the effects of graphene nanoparticles on the strain energy release rate and delamination growth of carbon-epoxy composites. It is expected that the significant improvements in G_{IC} that graphene contributes in neat epoxy will also greatly enhance the resistance to delamination in CG-Ep samples. To examine the strain energy release rate of C-Ep and CG-Ep specimens, double cantilever beam (DCB) testing will be utilized.

2. Materials and Specimen Preparation

The materials utilized in this study included all constituents of carbon/epoxy and graphene-carbon/epoxy composites, namely epoxy resin, carbon fiber, and graphene nanoparticles. EPON 862 epoxy resin cured with EPIKURE 3234 curing agent was used as the matrix material for both C-Ep and CG-Ep samples. Unidirectional carbon fiber (12K, Fiberglass Developments Corp.) was also utilized in both specimen types. For CG-Ep specimens, 99.9% pure graphene nanopowder with an average thickness of 8nm (20-30 graphene layers) was integrated into epoxy matrix.

Prior to fiber layup, graphene/epoxy matrix was prepared following a method outlined in Figure 1. Steps included in this process are: (a) - graphene nanopowder combined with acetone via mechanical mixing; (b) - graphene-acetone solution sonicated via VXC 750 model tip sonicator for 30 minutes; (c) - epoxy resin combined with graphene-acetone solution via mechanical mixing; (d) - graphene-epoxy-acetone solution sonicated for 60 minutes; (e) - graphene-epoxy-acetone solution subjected to constant heating (60°C) and constant magnetic stirring until acetone is removed from solution; (f) - curing agent combined with graphene-epoxy solution and mixed via high shear mixing (Thinky ARE-310 mixer) for 2 minutes; (g) - graphene-epoxy solution poured onto glass mold and allowed to cure for 24 hours at room temperature.

Finished carbon fiber reinforced composite panels were fabricated via a manual layup method. Carbon fiber fabric was cut to desired dimensions (30.5cm by 30.5cm) and layered to attain the desired specimen thickness (3.81mm). A manual layup approach was chosen to minimize filtration effects common to resin infusion techniques and to maximize dispersion of graphene nanoparticles throughout the specimen. Matrix material for each specimen type was manually applied to each layer of carbon fiber fabric (10 layers). To develop initial crack for DCB testing samples, a Teflon-coated release film layer was inserted between layers 5 and 6 for each panel. Once manual layup was complete, panels were covered and subjected to vacuum and positive pressure throughout the 24 hour curing process. Panels under vacuum pressure and completed panels are shown in Figure 2.

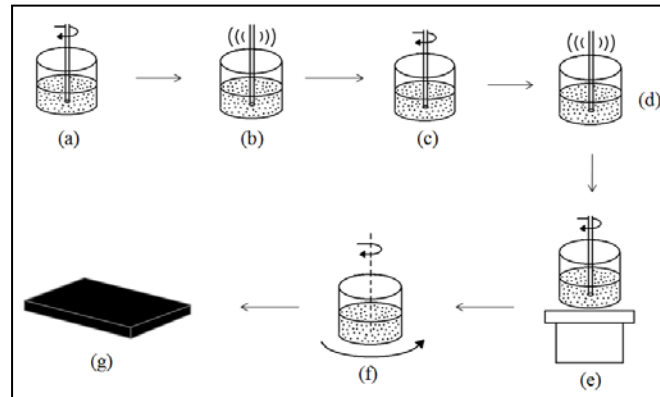


Fig. 1. Graphene-epoxy dispersion process.

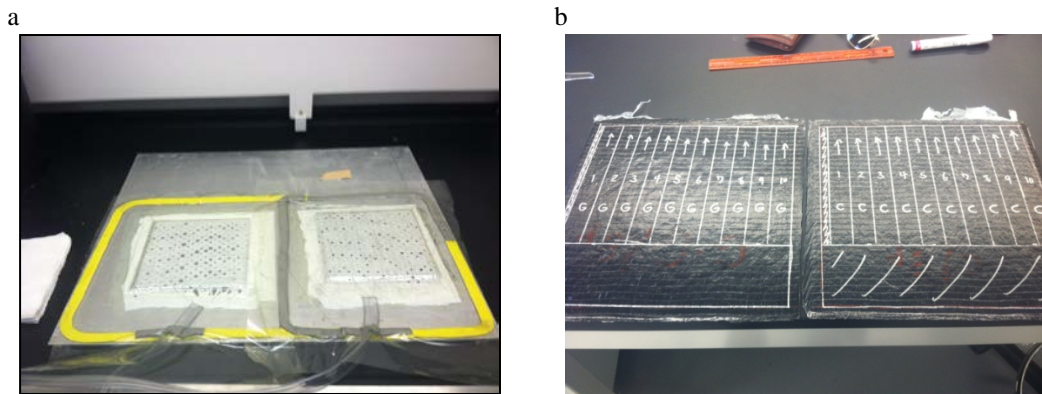


Fig. 2. (a) Panels curing under vacuum pressure; (b) Fabricated carbon fiber panels with specimen outlines.

Each panel was cut to produce 10 DCB specimens, with each specimen having dimensions of 20.32cm by 2.54cm by 0.381cm. To prepare individual DCB specimens, piano hinges were attached to the end of each specimen with industrial adhesive under clamping pressure. The sides of each specimen were marked to ensure precise tracking of crack growth under testing conditions.

3. Testing Method

As outlined earlier, double cantilever beam (DCB) testing was carried out for both C-Ep and CG-Ep specimens. DCB testing is a well known test procedure and has been utilized in many academic studies [9]. DCB tests consist of applying tensile load on each side of a single sample with some initial crack length(a) as shown in Figure 3.. The general test set-up and crack opening displacement (COD) of a DCB specimen is shown in Figure 4. DCB tests were conducted under displacement-controlled conditions using an electromechanical testing machine (QTEST/25 manufactured by MTS Systems Corp.) with constant cross head speed of 5.0 mm/minute to achieve stable delamination growth. DCB tests were carried out in accordance with specifications outlined in ASTM D5528 [10].

DCB tests produced load-displacement curves vital to the calculation of critical strain energy release rate, G_{IC} , via the compliance, C , of each specimen. At the onset of delamination growth, the load and total opening displacement, P_{cr} and δ_{cr} respectively, were recorded and used to calculate the compliance for that initial crack length using Equation 1.

$$C = \delta / P \quad (1)$$

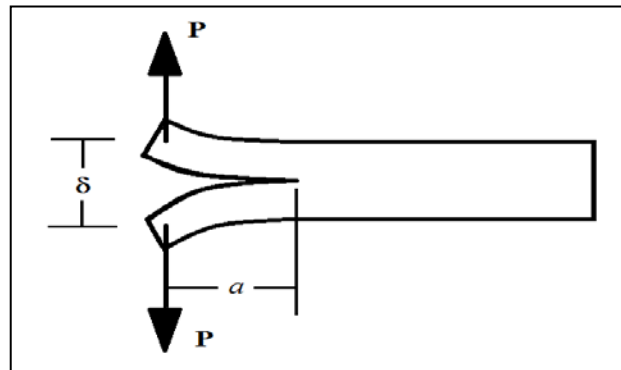


Fig. 3. Double cantilever beam loading.

Static DCB testing was conducted for several initial crack lengths, and compliance for each test data was recorded and compiled as a function of initial crack length. Using critical load and compliance as a function of initial crack length, along with specimen width (w), critical strain energy release rate can be calculated using Equation 2.

$$G_{IC} = \frac{P_{cr}^2 (dC/da)}{2w} \quad (2)$$

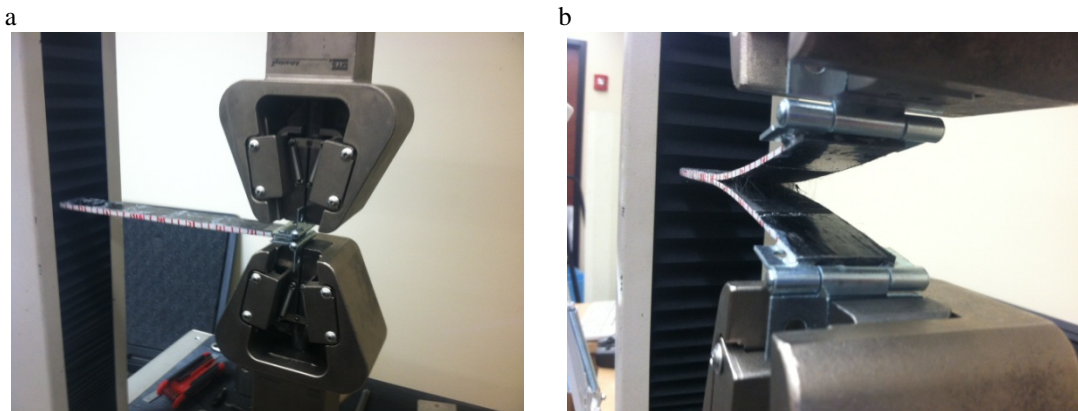


Fig. 4. DCB testing setup before (a) and during (b) loading of DCB specimens.

4. Results and Discussion

Static DCB testing was run for a number of initial crack lengths for both carbon-epoxy and 0.1% weight percentage carbon-graphene/epoxy specimens. Results were recorded and compiled for use in calculating the strain energy release rate of each sample type. The load vs. crack opening displacement chart for C-Ep specimen with various initial crack length is shown in Figure 5 as a reference. Similar plots were also generated for CG-Ep specimen. Samples were gradually loaded until the critical load limit was reached, then unloaded. This loading cycle was repeated for each initial crack length to produce a reliable delamination profile for each DCB specimen.

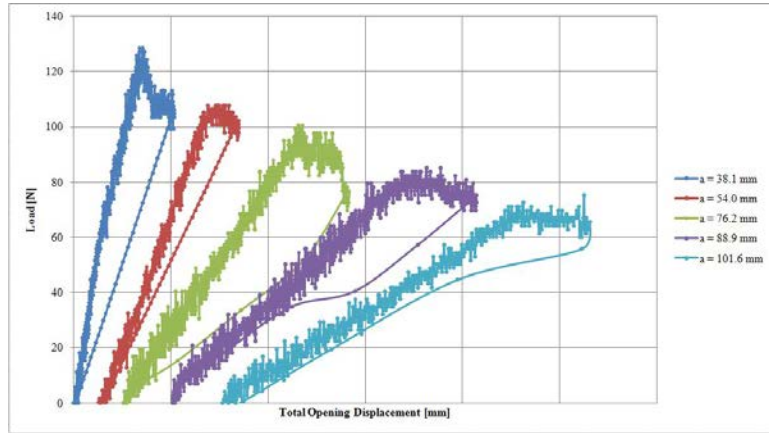


Fig. 5. Load vs. Displacement Plot for Static DCB Testing for C-Ep

The results of the DCB testing were quite promising. Data recorded during testing was plotted and a curve fit was applied to the relevant data points. These curve fits were substituted into Equation 2 to obtain strain energy release rate for each specimen type. Compliance vs. initial delamination and critical load vs. initial delamination length plots for C-Ep and C-G/Ep specimens are shown in Figure 6. It is seen that compliance increases and critical load decreases with increased delamination length.

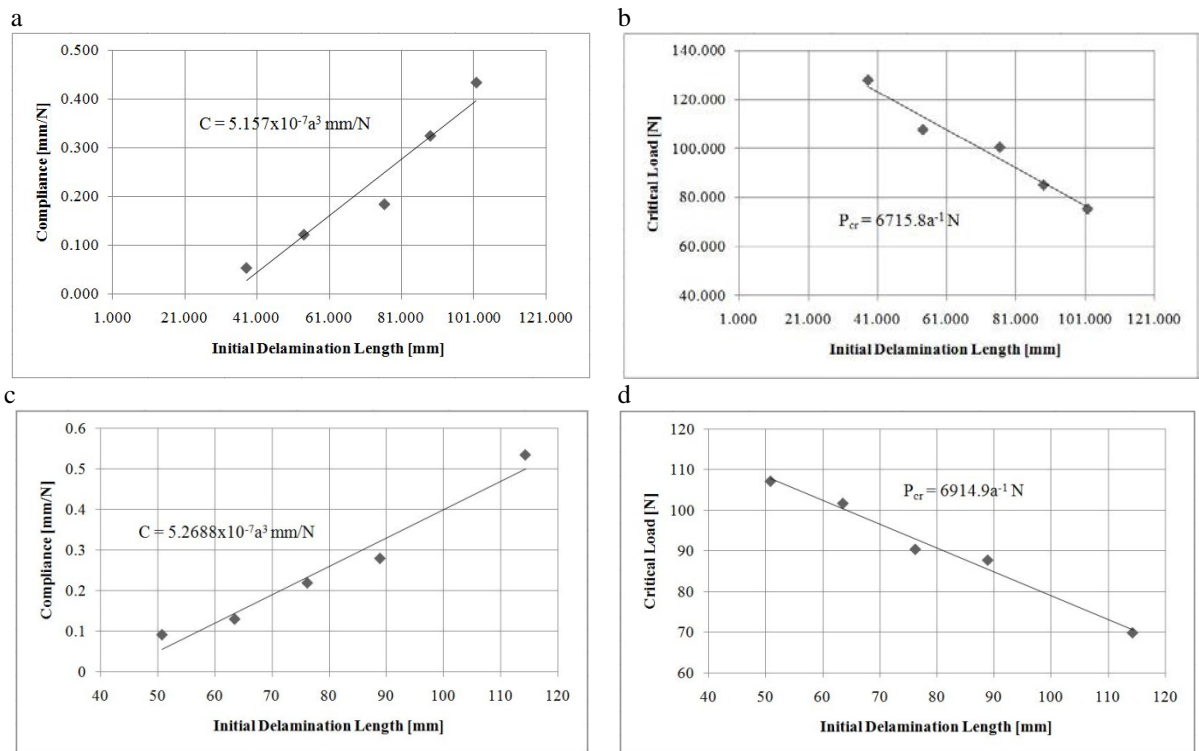


Fig. 6. (a) Compliance vs. Initial Delamination Length and (b) Critical Load vs. Initial Delamination Length for C-Ep DCB and (c) Compliance vs. Initial Delamination Length and (d) Critical Load vs. Initial Delamination Length for C-G/Ep DCB

Table 1. Strain Energy Release Rate

Specimen Type	G_{IC}	Percent Difference
[-]	[J/m ²]	[%]
Carbon-Epoxy	137.36	-
Carbon-Graphene/Epoxy	148.76	8.30

From experimental data, strain energy release rate of CG-Ep was calculated to be 148.76 J/m², compared to the same as 137.36 J/m² in conventional C-Ep specimens as shown in Table 1. Overall, this results show an improvement (8.3%) in strain energy release rate over that of conventional C-Ep specimens. Such results are comparable with G_{IC} value, 102.6 J/m² determined for carbon/epoxy (T300/5208) composites using a DCB specimen [4]. The discrepancy in this case is mostly due to different types of carbon fiber and epoxy resin used in T300/5208 system.

Conclusion

The critical strain energy release rate, G_{IC} , of graphene reinforced three phase carbon/epoxy hybrid composites has been evaluated using DCB specimen. The results show an increased G_{IC} in CG-Ep composites in comparison to conventional C-Ep composites. It is to be noted that a significant improvement (125%) in G_{IC} is reported for two phase graphene/epoxy (G-Ep) system [2] but such improvement is not observed in graphene reinforced three phase CG-Ep hybrid composites. Microscopic examinations show presence of graphene agglomeration in the system. It may be further enhanced adopting a more effective graphene dispersion method. Future work is focussed in dispersion of graphene in acetone through sonication and spraying acetone/graphene solution on each layer carbon fiber. It might provide uniformly dispersed exfoliated graphene in each fiber layer. Theoretical analysis for predicting critical strain energy release rate in CG-Ep, DCB specimen is in progress using analytical and finite element method for further understanding of mode-I delamination crack growth in laminated composites.

Acknowledgements

The authors would like to acknowledge the support of NSF grant EPS 1158862 for this study.

References

- [1] S. Tkachev, E. Buslaeva, S. Gubin, Graphene: A novel carbon nanomaterial, *Inorg. Mater+*, vol. 47, pp. 1-10, 2011.
- [2] M.A. Rafiee, J. Rafiee, I. Srivasta, Z. Wang, H. Song, Zhong-Zhen Yu, N. Koratkar, *Fracture and Fatigue in Graphene Nanocomposites*, Small, vol. 6, pp. 179-183, 2010.
- [3] M.J Laffan, S.T. Pinho, P. Robinson, A.J. McMillan, *Translaminar fracture toughness testing of composites: A review*, *Polymer Testing*, vol. 31, pp. 481-489, 2012.
- [4] R.L. Ramkumar, *Performance of a Quantitative Study of Instability-Related Delamination Growth*, NASA Contractor Report 166046, March 1983.
- [5] E. Bekyarova, E. T. Thostenson, A. Yu, H. Kim, J. Gao, J. Tang, H. T. Hahn, T.-W. Chou, M. E. Itkis, R. C. Haddon, *Multiscale Carbon Nanotube – Carbon Fiber Reinforcement for Advanced Epoxy Composites*, *Langmuir*, vol. 23, pp. 3970-3974, 2007.
- [6] K.L. Kepple, G.P. Sanborn, P.A. Lacasse, K.M. Gruenberg, W.J. Ready, *Improved fracture toughness of carbon fiber composite functionalized with multi walled carbon nanotubes*, *Carbon*, vol. 46, pp. 2026-2033, 2008.
- [7] Yuan Xu, Suong Van Hoa, *Mechanical properties of carbon fiber reinforced epoxy/clay nanocomposites*, *Compos. Sci. Technol.*, vol. 68, pp. 854-861, 2008.
- [8] R. Rahman, D.A. Hawkins Jr., D. Donewar, A. Haque, *Mechanical, Thermal, and Electrical Properties of Graphene/Epoxy Nanocomposites: An Experimental and Theoretical Study*, American Society for Composites 28th Technical Conference, 2013.
- [9] J.J.L. Morias, M.F.S.F. De Moura, F.A.M. Pereira, J. Xavier, N. Dourado, M.I.R. Dias, J.M.T. Azevedo, *The double cantilever beam test applied to mode I fracture characterization of cortical bone tissue*, *Journal of the Mechanical Behavior of Biomedical Materials*, vol. 3, pp. 446-453, 2010.
- [10] ASTM Standard D5528, 2013, *Standard Test Methods for Mode I Interlaminar Fracture Toughness of Unidirectional Fiber-Reinforced Polymer Matrix Composites*, ASTM International, West Conshohocken, PA, 2013.



6th BSME International Conference on Thermal Engineering (ICTE 2014)

Pressure distributions and forces on hexagonal cylinder

Kapil Ghosh^{a*}, Md. Quamrul Islam^a, Mohammad Ali^a

^a Department of Mechanical Engineering, Bangladesh University of Engineering and Technology (BUET), Dhaka-1000, Bangladesh

Abstract

In this research work, an experimental investigation of wind effect on hexagonal cylinder was carried out. The study was performed on the single cylinder. The test was conducted in an open circuit wind tunnel at a Reynolds number of 4.22×10^4 based on the face width of the cylinder across the flow direction in a uniform flow velocity of 13.5 m/s. The test was carried out at various angles of attack from 0° to 50° at a step of 10° . The surface static pressures at the different locations of the cylinder were measured with the help of inclined multi-manometers. The wind velocity was kept constant at 13.5 m/s. The pressure coefficients were calculated from the measured values of the surface static pressure distribution on the cylinder. Later the drag and lift coefficients were obtained from the pressure coefficients by the numerical integration method. The results will enable the engineers and architects to design buildings more efficiently. Since the results will be expressed in the non-dimensional form they may be applied for the prototype building.

© 2015 The Authors. Published by Elsevier Ltd.

Peer-review under responsibility of organizing committee of the 6th BSME International Conference on Thermal Engineering (ICTE 2014).

Keywords: Drag coefficient; Lift coefficient; Hexagonal cylinder; Pressure distribution; Wind load.

1. Introduction

The subjects of wind load on buildings and structures are not a new one. In the 17th century, Galileo and Newton have considered the effect of wind loading on buildings, but during that period, it did not gain popularity. The effect of wind loading on buildings and structures has been considered for design purposes since late in the 19th century; but starting from that time up to about 1950, the studies in this field have not been considered seriously. Building and their components are to be designed to withstand the code specified wind loads. Calculating wind

* Corresponding author. Tel.: +8801723471067.

E-mail address: kapil_chaity@yahoo.com

loads is important in the design of wind force resisting system, including structural members, components, and cladding against shear, sliding, overturning, and uplift actions. In recent years, much emphasis has been given on “The study of wind effect on buildings and structures” in the different corners of the world. Even researchers in Bangladesh have taken much interest in this field. Till now, little attention has been paid to the flow over the bluff bodies like square cylinders, rectangular cylinders, octagonal cylinders etc. and some information is available concerning the flow over them in staggered condition, although this is a problem of considerable practical significance. With the progressing world, Engineering problems regarding wind loads around a group of skyscrapers, chimneys, towers and the flow induced vibration of tubes in heat exchangers, bridges, oil rigs or marine structures need detailed investigation of flow patterns and aerodynamic characteristics. Arising from the increasing practical importance of bluff body aerodynamics, over the past few decades’ sufficient effort has been given in research works concerning laboratory simulations, full-scale measurements and more recently numerical calculations and theoretical predictions for flows over bodies of wide variety of shapes. A number of failures of bridges, transmission towers, buildings and housings over the last one hundred years prompted researchers to do research work in this field.

It is the great challenge of the engineers and architects to reduce the wind load on the tall buildings. Nowadays due to huge population pressure, emphasis on design and construction of the tall buildings is being given in many places. Especially the design of the group of tall buildings is the most important consideration to take care of the housing problem of the huge population. As the building becomes tall it is necessary to take into consideration the effect of wind on its design. Keeping this in mind the study on the hexagonal cylinder has been conducted, which will be applicable to obtain the wind load on the tall buildings. The study of wind effect was first limited to loading on buildings and structures only, possibly because of its most dramatic effects are seen in their collapses. In mid-sixties, researchers started the study of less dramatic, but equally important environmental aspects of flow of wind around buildings. These include the effects on pedestrians, weathering, rain penetration, ventilation, heat loss, wind noise and air pollution etc. The pioneer researcher in this field is Lawson, T.V. [1] of the University of Bristol. A number of works of the environmental aspects of wind was being studied at the Building Research Establishment at Garson and the University of Bristol, UK.

It is true that researchers from all over the world have contributed greatly to the knowledge of flow over bluff bodies as published by Mchuri, F. G. [2] but the major part of the reported works are of fundamental nature involving the flow over single body of different profiles. Most of the researchers have conducted works either on single cylinder with circular, square, octagonal or rectangular sections etc. or in a group with them for various flow parameters. However, the flow over a hexagonal cylinder has not been studied extensively, although this is a problem of practical significance. It is believed that the study on the cylinder with hexagonal section will contribute to find the wind load on the single hexagonal building and the results will be useful to the relevant engineers and architects. There are various parameters, which control the flow behavior as mentioned by Castro, J.P. [3]. They are (i) vortices in front of the building, (ii) opening through buildings, (iii) spacing of rows, (iv) wakes of buildings, (v) long straight streets, (vi) narrowing streets; (vii) corners and (viii) courtyards. The mean wind speed varies with height. The variation of wind speed has been expressed by Davenport, A. G. [4]. The wind in the atmospheric boundary layer varies in time and space. The source of wind energy is the sun that emits solar radiation, which causes differential heating of the earth surface and the atmosphere.

In the atmosphere there is a general convective transport of heat from lower to higher latitudes in order to make the earth's radiation imbalance as mentioned by Lanoville, A. [5]. It is for this reason that the atmosphere is a restless medium in which circulation of all sizes is normal. Lee [6] performed study on the effect of turbulence on the surface pressure field on a square prism. In his study, measurements were presented of the mean and fluctuating pressure field acting on a two dimensional square cylinder in uniform and turbulent flows. In his investigation he showed that the addition of turbulence reduces the drag on the cylinder. Mandal and Farok [7] measured the static pressure distributions on the single cylinder with square and rectangular cross-section having rounded corners in a uniform cross flow. The experiment was conducted for different corner radii and side dimensions of the cylinders at

zero angle of attack. The experimental results reveal that the corner radius of the cylinder has significant effect while the side dimension has some effect on the drag coefficient. Mandal and Islam [8] made an experimental investigation of mean pressure coefficients on square cylinders. They measured the pressure coefficients on single square cylinder at various angles of attack and on a group of square cylinders with sharp edge at zero angle of attack. Islam and Mandal [9] performed an experimental investigation of static pressure distributions on a group of rectangular cylinders in a uniform cross flow. The effect of longitudinal spacing as well as the side dimension of the cylinder was taken into consideration in the study.

It is the task of the engineer to ensure that the performance of structures subjected to the action of wind will be adequate during their anticipated life from the standpoint of both structural safety and serviceability. To achieve this end, the designer needs information regarding (i) the wind environment, (ii) the relation between that environment and the forces it induces on the structures, (iii) the behavior of the structure under the action of forces. The knowledge of wind loading on a single tall building or on a group of tall buildings is essential for their economic design. The flow around a hexagonal model cylinder can be ideally considered analogous to that of the flow around a tall hexagonal-shaped building. Therefore, a study of wind flow around hexagonal cylinder would be helpful in this respect. The wind in the atmospheric boundary layer varies in time and space. It depends on the terrain roughness, the local wind climate and on variations in temperature. Usually the effects of temperature are assumed negligible, when studying wind loads relevant are the proper simulation of the wind speed with height and the turbulent characteristics. Though the problem regarding the wind loadings on buildings and structures is common to all parts of the world and it is expected that the solution will not be significantly different from country to country, yet research work should be carried out in this field considering the climatic conditions and problem of this country so that a clear picture about the nature of wind loading can be obtained. The data from these research works should enable to the architects, engineers and town planners of Bangladesh to design buildings and structures more efficiently.

Nomenclature

A	Frontal area of the Cylinder
F_D	Drag force
F_L	Lift force
C_L	Coefficient of lift
C_D	Coefficient of drag
C_p	Coefficient of pressure
ρ	Density of the air
U_∞	Free stream velocity
ΔP	Pressure difference
Δh_w	Manometer reading
γ_w	Specific weight of manometer liquid (water)
α	Angle of attack
V	Wind speed
Z	Height
dp/dn	The pressure gradient
P	Pressure on the surface of the cylinder
P_0	The ambient pressure
h_a	The air head
γ_a	The specific weight of air

2. Experimental set-up

2.1. Wind tunnel

The test was conducted at the exit end of an open circuit subsonic wind tunnel. In Figure 1 the schematic diagram of the wind tunnel is presented showing the position of the cylinder at the exit end of the wind tunnel in a uniform cross flow. The wind tunnel was 5.93 m long with a test section of 460 mm x 460 mm cross section. The cylinder was fixed to the side walls of the extended portion at the exit end. In the side wall the cylinder was fastened rigidly at one end and through the other end of the cylinder the plastic tubes from the tapping were taken out and were connected with the inclined multi-manometer, which contained water as the manometer liquid. The cylinder was levelled in such a way that the top and bottom face of the hexagonal cylinder was parallel to the flow direction. The axis of the cylinder was at the same level to that of the wind tunnel. To generate the wind velocity, two axial flow fans are used. Each of the fans is connected with the motor of 2.25 kilowatt and 2900 rpm. The induced flow through the wind tunnel is produced by two-stage rotating axial flow fan of capacity 18.16 m³/s at the head of 152.4 mm of water and 1475rpm. In each case of the tests, wind velocity is measured directly with the help of a digital anemometer. The flow velocity in the test section was maintained at 13.5m/s approximately. The measured velocity distribution was almost uniform across the tunnel test section in the upstream side of the test models.

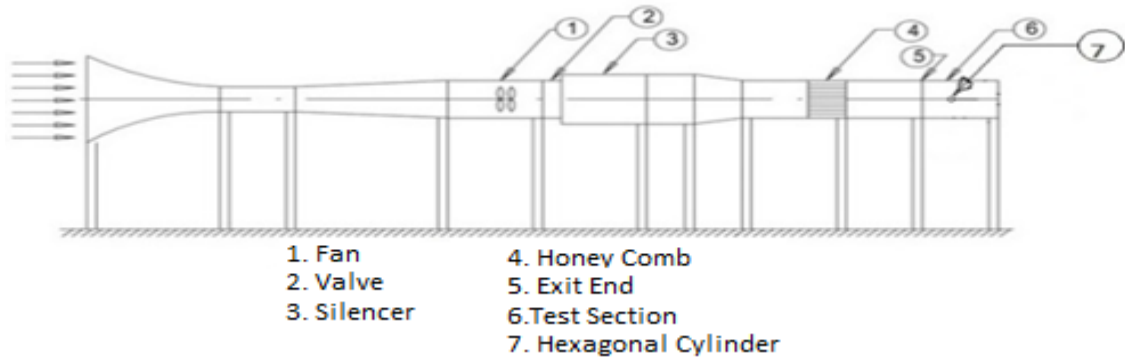


Fig.1. Schematic diagram of wind tunnel

The pattern of the flow velocity is shown in Figure 2 in the non-dimensional form. The values of U/U_∞ and h/H were matched with each other. The most obvious quantity that can be measured with the Pitot-static probe is the velocity distribution in the upstream side of the test models. The following figure shows the velocity distribution across the test section.

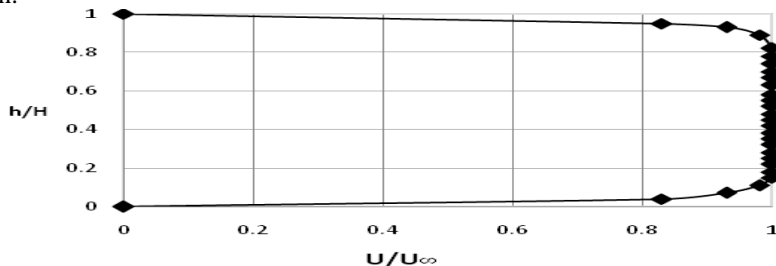
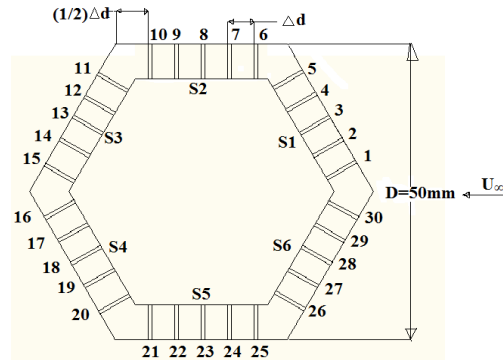


Fig.2. Velocity distribution at upstream side of model cylinder

There was a provision for rotation of the test cylinder at various angles to obtain the wind load at different angles of attack. The Reynolds number was 4.22×10^4 based on the projected width of the cylinder across the flow direction. Since the top and bottom of the extended part of the wind tunnel was open; as such no correction for blockage was done in the analysis. The test cylinders were placed very close to the end of the wind tunnel so that the approach velocity on the test cylinders was approximately identical as that in the exit end of the wind tunnel.

2.2. Constructional details of cylinders

The tapping positions on the cross-section of the cylinder are shown in Figure 3. The width of the hexagonal cylinder was 50mm as shown in the figure. Each face of the cylinder contained five tappings.



Hexagonal Cylinder

Fig.3. Tapping positions shown on cross-section of cylinder

In Figure 4 the tapping positions on the longitudinal section of the cylinder is shown. There were five tappings on each face of the cylinder. The distance between the consecutive tapping points was equal (Δd) as shown in the figure. However, the location of the corner tapping was at a distance of $\frac{1}{2}\Delta d$. Each tapping was identified by a numerical number from 1 to 30 for hexagonal cylinder as can be seen from the figure. It can be seen from the longitudinal section that the tappings were not made along the cross-section of the cylinder. They were located within some span of the cylinder as shown in Figure 4. On one side of the cylinder a steel plate was attached through which there was a bolt for fixing the cylinder with the side wall of the extended tunnel as shown in Figure 4. The other side of the cylinder was hollow through which the plastic tubes were allowed to pass. The plastic tubes were connected with the copper capillary tubes at one side and at the other side with the inclined multi-manometer. The manometer liquid was water. The tappings were made of copper tubes of 1.71 mm outside diameter. Each tapping was of 10 mm length approximately. From the end of the copper tube flexible plastic tube of 1.70 mm inner diameter was press fitted.

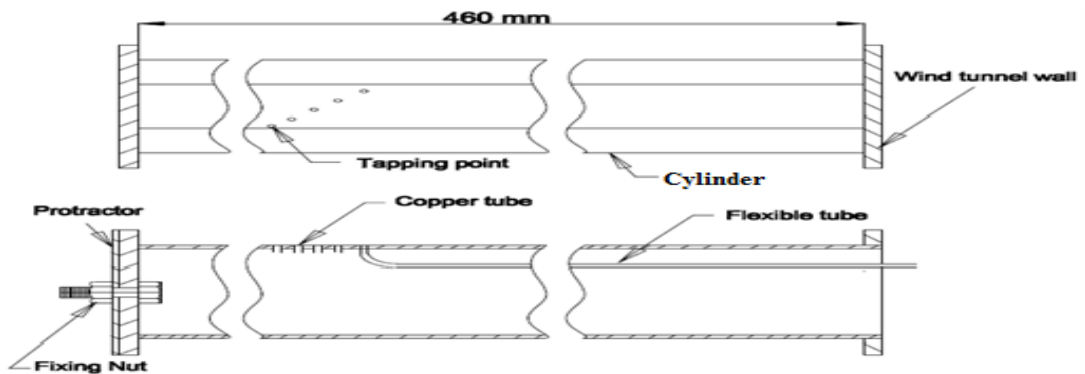


Fig.4. Tapping positions shown on longitudinal section of cylinder

The upstream velocity was assumed to be uniform and the flow occurred across the cylinder. In Figure 5 the position of the single cylinder at zero angle of attack is shown in the wind tunnel test section. The surface static pressure distributions on faces of the cylinder were measured in this position. Then the cylinder was rotated at an angle of 10° for hexagonal cylinder and the static pressure distributions on each face of the cylinder were measured again. The same test procedure was repeated to measure the surface static pressure distributions of the cylinders with angles of attack of $0^\circ, 10^\circ, 20^\circ, 30^\circ, 40^\circ$ and 50° for hexagonal cylinder.

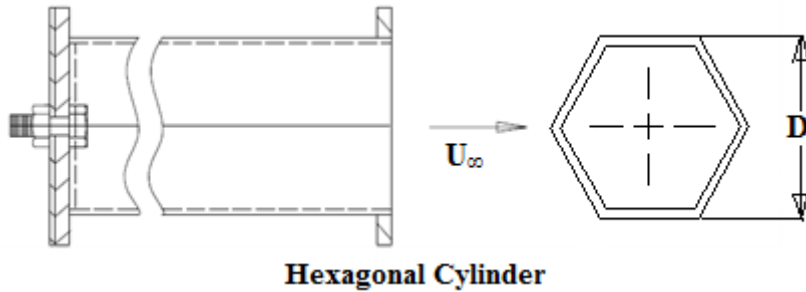


Fig.5. Tunnel test section showing position of single cylinder

3. Mathematical Model

The pressure coefficient is defined as

$$C_P = \frac{\Delta P}{\frac{1}{2} \rho U_\infty^2} \quad (1)$$

Drag and lift coefficients are defined as follows

$$C_D = \frac{F_d}{\frac{1}{2} \rho A U_\infty^2} \quad (2)$$

$$\text{and } C_L = \frac{F_L}{\frac{1}{2} \rho A U_\infty^2} \quad (3)$$

4. Results and Discussion

4.1. Distribution of pressure coefficients on hexagonal cylinder

The cross-section of the single hexagonal model cylinder with 30 numbers of tappings, five numbers on each surface of the cylinder at an angle of attack has been shown in Figure 3. The six surfaces have been identified with S_1, S_2, S_3, S_4, S_5 and S_6 . Pressure coefficient for each tapping point has been determined from the measured surface static pressure. In Figures 6 to 11, the distributions of static pressure coefficients for angles of attack of 0° to 50° with a step of 10° have been presented respectively. From Figure 6 one can observe that the distribution of the pressure coefficients is symmetric at zero angle of attack. It can be further noticed from this figure that there is no stagnation point. It is due to the fact that the location at the stagnation point has not been selected for the tapping. The pressure coefficient values are positive on the surfaces S_1 and S_6 , while on the surfaces S_2 to S_5 there are negative pressure coefficients. However, one interesting point can be seen from this figure that almost uniform pressure coefficient distributions are found on surfaces S_2 to S_5 . In Figure 7 at angle of attack of 10° , the value of the pressure coefficient has increased slightly on surface S_1 , while it has dropped slightly on surface S_6 . However, on the other four surfaces S_2 to S_5 , the distributions of pressure coefficient are almost uniform. At $\alpha = 10^\circ$, the C_p -distribution is close to that at $\alpha = 0^\circ$. In Figure 8 at angle of attack of 20° , there is further rise of C_p values on surface S_1 and further drop of C_p values on surface S_6 . However, on surfaces S_3 to S_5 almost uniform C_p -distribution occurs. While on surface S_2 there is high suction near the tapping point 6. Probably, the shear layer deviates much in the

outward direction near this point. At $\alpha = 30^\circ$, an interesting point can be observed from Figure 9, where on surface S_1 , there is stagnation point on tapping point 3. The distributions of C_p on surfaces S_2 and S_6 are symmetric, which is expected at this angle of attack. On surfaces S_2 and S_6 near the tapping points 6 and 30 respectively, there are high suction, which indicates the high deviation of the shear layer in the outward direction from the body, while reattachment is seen to occur at the downstream side of the surfaces S_2 and S_6 . However, there is almost uniform C_p -distribution on the surfaces S_3 to S_5 . It is observed from Figure 10 that, there is still stagnation point on surface S_1 , but it occurs at tapping point 4. Due to further rotation the surface S_2 shows positive values of C_p . However, on the surfaces S_3 to S_5 , there is more or less uniform distribution of C_p . While on surface S_6 the C_p values become less negative. There appears reattachment near the tapping point 27 on the surface S_6 . Finally, from Figure 11 at $\alpha = 50^\circ$, it is seen that the stagnation point still occurs at tapping point 4 and there is further rise of positive C_p values on the surface S_2 and all values are positive on this surface. On the surfaces S_3 to S_5 , the C_p values are more or less uniform. While on the surface S_6 , there is very high suction. Further rotation of the cylinder has not been made because at $\alpha = 0^\circ$ and $\alpha = 60^\circ$, they are identical.

4.2. Variation of drag coefficient on hexagonal cylinder

Variation of drag coefficient at various angles of attack on single hexagonal cylinder is shown in Figure 12. The drag coefficient at different angles of attack on a single square cylinder at uniform flow obtained by Mandal, A. C. [7] is also presented in this figure for comparison. It can be noticed from this figure that there is significant drop in the drag coefficient values for the hexagonal cylinder in comparison to that of the square cylinder and the values approach to that of the circular cylinder. It is seen from this figure that at zero angle of attack, the drag coefficient is about 0.95 and at all other angles of attack, the values are close to 0.80 except at angle of attack of 10° , where the value is about 0.50. The values of the drag coefficient at various angles of attack for the hexagonal cylinder can be explained from the C_p -distribution curves.

4.3. Variation of lift coefficient on hexagonal cylinder

In Figure 13 the variation of lift coefficient at various angles of attack on single hexagonal cylinder is shown. The lift coefficient at different angles of attack on a square cylinder at uniform flow obtained by Mandal, A. C. [7] is also presented in this figure for comparison. It can be noticed from this figure that the variation of the lift coefficient on the single hexagonal cylinder is not appreciable; they are close to zero value except at angles of attack of 10° and 50° , where some insignificant values are observed. For the single square cylinder the variation of lift coefficient with angle of attack is remarkable. The values of the lift coefficients for the single hexagonal cylinder can be explained from the C_p -distribution curves.

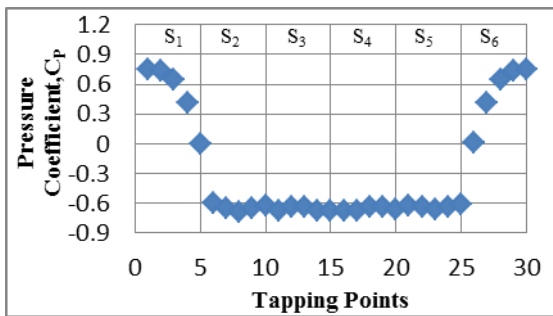


Fig.6. Distribution of Pressure Coefficient on Hexagonal Cylinder at Angle of Attack of 0°

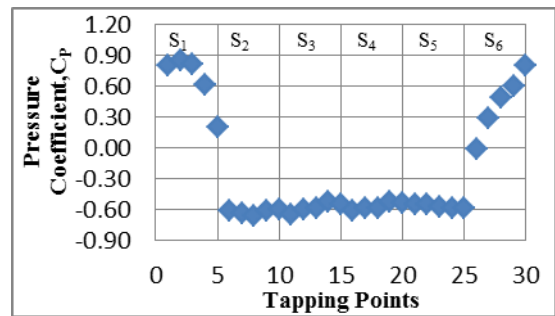


Fig.7. Distribution of Pressure Coefficient on Hexagonal Cylinder at Angle of Attack of 10°

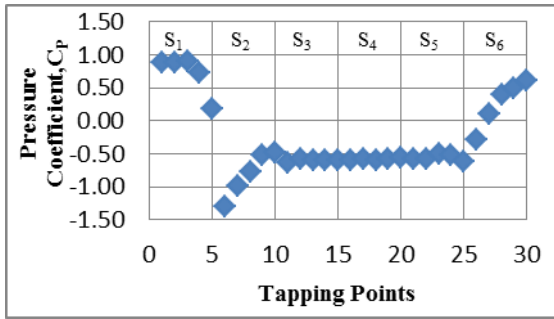


Fig.8. Distribution of Pressure Coefficient on Hexagonal Cylinder at Angle of Attack of 20°

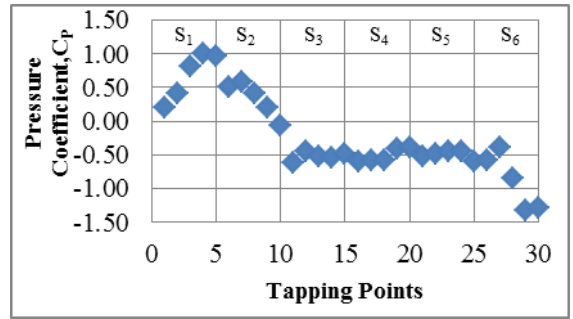


Fig.11. Distribution of Pressure Coefficient on Hexagonal Cylinder at Angle of Attack of 50°

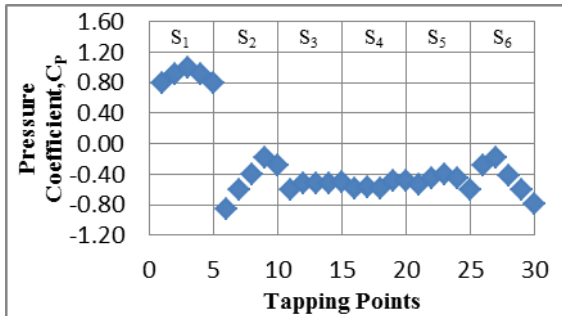


Fig.9. Distribution of Pressure Coefficient on Hexagonal Cylinder at Angle of Attack of 30°

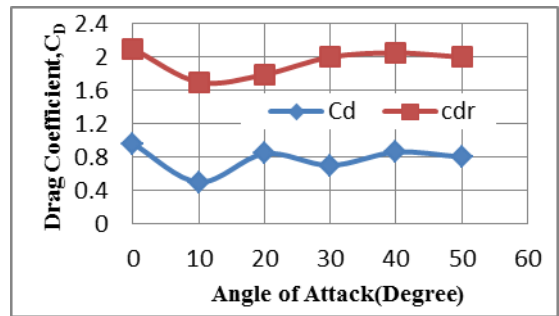


Fig.12. Variation of Drag Coefficient at Various Angles of Attack on Single Hexagonal Cylinder

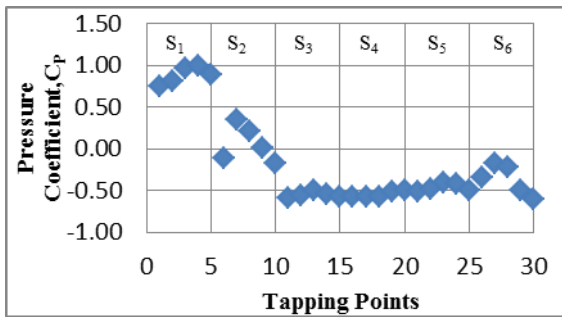


Fig.10. Distribution of Pressure Coefficient on Hexagonal Cylinder at Angle of Attack of 40°

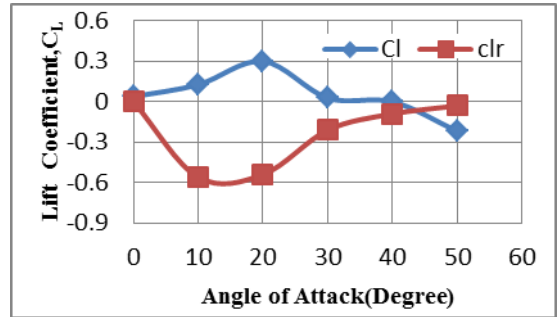


Fig.13. Variation of Lift Coefficient at Various Angles of Attack on Single Hexagonal Cylinder

5. Conclusion

The following conclusions are drawn in regard to the wind effect on the single hexagonal cylinder. There is significant drop in the drag coefficient values for the single hexagonal cylinder in comparison to that of the single square cylinder and the values approaches to that of the circular cylinder. The drag coefficient for a single hexagonal cylinder at zero angle of attack is about 0.95 in contrast to that of 2.0 for a single square cylinder at the same angle of attack. The variation of the lift coefficient on the single hexagonal cylinder is not appreciable and they are close to zero value except at angles of attack of 10° and 50° , where some insignificant values are observed. The stagnation point is found on the front face of the single hexagonal cylinder. While wind load is to be used for the design of the free-standing building having hexagonal cross-section, the outcome of the present results may be applied.

Acknowledgements

This research work was funded by Department of Mechanical Engineering, Bangladesh University of Engineering & Technology.

References

- [1] Lawson, T.V., “Wind Loading of Buildings, Possibilities from a Wind Tunnel Investigation”, University of Bristol, U.K. Report on TVL /731A, August, 1975.
- [2] Mehuri, F.G. et al, “Effects of the free Stream Turbulences on Drag Coefficients of Bluff sharp- Edged Cylinders”, *Nature*, Vol.224, No. 5222, November 29, 1969,pp. 908-909.
- [3] Castro, J.P. and Fackwell, J.E., “A Note on Two- Dimensional Fence Flows with Emphasis on Wall Constant”, *J. Industrial. Aerodynamics*, 3(1), March1978.
- [4] Davenport, A.G., “The Relation to wind Structure to Wind Loading” “Proceedings of the Conference on Wind Effects on Buildings and Structures”, Vol.1, June, 1963.
- [5] Lanoville, A., Gateshore, I.S. and Parkinson, G.V., “An Experimental of some effects of turbulence on bluff bodies”, *Proceeding of the 4th international Conference on wind Effects on Buildings and Structure*, London, U.K.1975, pp.333-341.
- [6] Lee, B.E., “The Effect of Turbulence on the Surface Pressure Field of a Square Prism”, *Journal of Fluid Mechanics*, Vol.6 J.E. 9, Part 2, 1975, pp. 263-282.
- [7] Mandal, A.C. and Farok, G.M.G., “An Experimental Investigation of Static Pressure Distributions on Square and Rectangular Cylinders with Rounded Corners”, 4th International Conference on Heat Transfer, Fluids Mechanics and Thermodynamics (HEFAT), Cairo, Egypt, September. 2005, Cairo, Egypt, Paper NO. : MA5.
- [8] Islam, A.T.M. and Mandal, A.C., “Experimental Analysis of Aerodynamic Forces for Cross- flow on single Rectangular Cylinder”, *Mechanical Engineering Research Bulletin, BUET, Dhaka*, Vol.13, No.1, 1990, pp. 36-51.
- [9] Islam, A.M.T. and Mandal, A.C., “Static Pressure Distribution for Cross- flow on single Rectangular Cylinders”, *Mechanical Engineering Research Bulletin, BUET, Dhaka*, Vol.14, No.1, 1991, pp.8-23.